



## Geochemical responses of scleractinian corals to nutrient stress

C.D. Standish <sup>a,\*</sup>, T.B. Chalk <sup>a,b</sup>, M. Saeed <sup>a</sup>, F. Lei <sup>c</sup>, M.C. Buckingham <sup>a</sup>, C. D'Angelo <sup>a</sup>, J. Wiedenmann <sup>a</sup>, G.L. Foster <sup>a</sup>

<sup>a</sup> School of Ocean & Earth Sciences, University of Southampton, National Oceanography Centre, European Way, Southampton, SO14 3ZH, UK

<sup>b</sup> Aix Marseille Univ, CNRS, IRD, INRAE, CEREGE, Aix-en-Provence, France

<sup>c</sup> School of Geography and Ocean Science, Nanjing University, Nanjing 210023, China



### ARTICLE INFO

Associate editor: Claire Rollion-Bard

**Keywords:**  
Coral  
Nutrients  
Element/Ca  
Boron isotopes

### ABSTRACT

The impact of changing nutrient conditions on scleractinian coral-based geochemical proxies is poorly understood, despite the nutrient balance in many coral reefs being disturbed by anthropogenic activity. Here, the geochemical responses of tropical corals *Acropora polystoma* and *Porites lichen* to nutrient enrichment and depletion are examined following growth under cultured conditions, to assess the impact of nutrients on traditional geochemical proxies for both temperature and the coral internal carbonate system. The corals were exposed to four different nutrient treatments over a period of 140 days: (1) a replete treatment with optimal levels of nitrate (~4.5 µM) and phosphate (~0.6 µM), (2) a nutrient depleted treatment with negligible nitrate and phosphate, (3) a treatment with high nitrate (~73 µM) and negligible phosphate, and (4) a treatment with high phosphate (~5.7 µM) and negligible nitrate. Results suggest nutrients play a hitherto under-appreciated role in coral skeleton elemental (Li/Ca, B/Ca, Mg/Ca, Sr/Ca, Li/Mg) and isotopic ( $\delta^{11}\text{B}$ ) composition, with the internal carbonate chemistry also impacted. For example, Mg/Ca and Sr/Ca are lower, and Li/Mg higher, in the nutrient imbalanced and deplete treatments compared to the replete treatment for both species. Disruption to the carbonate system in corals cultured under imbalanced nutrient conditions is best explained by a decrease in dissolved inorganic carbon flux to the extracellular calcifying medium. Variations in nutrient concentration — or nutrient imbalance — can have dramatic consequences on both reconstructed sea surface temperatures and ocean or calcification pH, with reconstructed temperatures varying from  $-7^\circ\text{C}$  to  $+52^\circ\text{C}$ , and  $\delta^{11}\text{B}$ -derived pH by up to 0.13 pH units. The impact from anthropogenically-induced nutrient disturbances should therefore be considered when generating temporal records of environments using coral skeletal archives.

### 1. Introduction

Scleractinian corals are important archives of environmental information, with the elemental and isotopic composition of their aragonite skeletons acting as sensitive environmental proxies for the waters in which they mineralised (Thompson, 2022) and/or as tracers of the carbonate system within their calcifying fluid (Krief et al., 2010; McCulloch et al. 2012a). In particular, the boron isotope ratio ( $\delta^{11}\text{B}$ ) is a well-established proxy for the pH of seawater (Hemming and Hanson, 1992) and is widely used in studies concerned with ocean acidification (e.g. Wei et al., 2009; Fowell et al., 2018, D'Olivo et al., 2019), whilst element to calcium ratios (E/Ca) such as Li/Ca, B/Ca, Mg/Ca, Sr/Ca, Ba/Ca, U/Ca and Li/Mg are employed as proxies for seawater temperature and salinity, as well as tracers for processes such as upwelling and terrestrial run-off (Lea et al., 1989; Beck et al., 1992; Mitsuguchi et al.,

1996; Sinclair et al., 1998; Watanabe et al., 2001; Fallon et al., 2003; McCulloch et al., 2003; Wei et al., 2009; Gaetani et al., 2011; Montagna et al., 2014; Cuny-Guirriec et al., 2019; Ross et al., 2019). Furthermore, when combined,  $\delta^{11}\text{B}$  and B/Ca enable investigations into the internal carbonate chemistry and calcification mechanisms of these organisms (Wall et al., 2019; Chalk et al., 2021). Together, they provide a powerful geochemical toolkit for oceanographic investigations (Thompson, 2022).

Nutrients, including nitrogen and phosphorous, are key for coral holobiont physiology, and play important roles in metabolic processes such as skeletal and tissue growth, as well as influencing zooxanthellae density and photosynthesis (Dubinsky and Jokiel, 1994; Marubini and Davies, 1996; Ferrier-Pagès et al., 2000; Houlbrèque et al., 2003; Houlbrèque and Ferrier-Pagès, 2009; Godinot et al., 2011). Being both auto- and heterotrophs, corals are able to exploit a range of nutritional

\* Corresponding author.

E-mail address: [c.d.standish@soton.ac.uk](mailto:c.d.standish@soton.ac.uk) (C.D. Standish).

pathways: nutrients may be acquired through heterotrophic feeding of detrital particulate organic matter or live organisms such as zooplankton and phytoplankton (Sorokin, 1991; Sebens et al., 1996; Houlbrèque and Ferrier-Pagès, 2009; Rosset et al., 2015), or they may be assimilated from dissolved inorganic nutrients via their symbiotic zooxanthellae (Crossland and Barnes, 1977; Muscatine and D'Elia, 1978; Grover et al., 2003; Godinot et al., 2009; Rosset et al., 2015).

A number of natural and anthropogenic drivers can alter the nutrient budget available to the coral holobiont (D'Angelo and Wiedenmann, 2014). Changes in upwelling and water mixing, sediment mobilisation (e.g. by storm activity), nitrogen fixation, and river runoff (delivering terrestrially derived nutrients) all play a role, and in some cases are seasonally-driven (Ullman and Sandstrom, 1987; Szmant and Forrester, 1996; Bell et al., 1999; Devlin and Brodie, 2005; Lapointe et al., 2019), with anthropogenic activities and processes such as the establishment of fish farms, sewage discharge, the use of fertilisers, deforestation, and other land-use transformations contributing to both changes in oceanic nutrient levels and eutrophication on coral reefs (Tomascik and Sander, 1987; Mitchell et al., 2001; Loya, 2004; Devlin and Brodie, 2005; Fabricius, 2005; DeGeorges et al., 2010; Brodie et al., 2012; Maina et al., 2012; Lapointe et al., 2019).

The response of coral physiology to nutrient enrichment is unclear in the literature. Some studies have revealed either an absence of negative effects, or even positive reactions, to increased nutrients concentrations (Koop et al., 2001; Szmant, 2002; Bongiorni et al., 2003; Dunn et al., 2012). Yet enrichment, or perhaps more specifically imbalanced enrichment of nutrients (i.e. enrichment of one specific nutrient), can also have a detrimental effect: reducing calcification rates and skeletal density (Stambler et al., 1991; Dunn et al., 2012), lowering reproductive success (Loya, 2004; Fabricius, 2005), damaging the coral-algal symbiosis (Dubinsky et al., 1990; Rosset et al., 2017; Becker and Silbiger, 2020), and increasing their susceptibility to episodes of bleaching when exposed to heat and light stress (Wiedenmann et al., 2013; DeCarlo et al., 2020). Furthermore, nutrient deprivation can also impair the functioning of the coral-algal symbiosis, as well as result in lower zooxanthellae density, smaller polyp sizes, and increased susceptibility to bleaching (Rosset et al., 2015). Therefore, whilst the relationship between nutrient levels and coral physiology is undoubtedly complex, it is clear that when certain nutrient thresholds are either exceeded or not reached, coral holobiont survival — and consequently coral reef resilience — can be severely impacted (D'Angelo and Wiedenmann, 2014). Despite this recognition of the effects of variable nutrient availability on coral physiology, their effects on biomineralisation mechanisms and associated skeletal elemental composition remain poorly constrained.

Elements may be incorporated into the calcium carbonate crystal lattice that form scleractinian coral skeletons via a variety of processes, such as direct cation substitution of  $\text{Ca}^{2+}$  (for  $\text{Sr}^{2+}$ ; Gaetani and Cohen, 2006), occlusion of organic-bound material (e.g.  $\text{Mg}^{2+}$ ; Finch and Allison, 2008), entrapment of cations by newly formed aragonite or at crystal defect sites ( $\text{Li}^+$  and  $\text{Mg}^{2+}$ ; Gabitov et al., 2011; Rollion-Bard and Blamart, 2015), or substitution into the mineral anion site of aragonite  $\text{CO}_3^{2-}$  (e.g.  $\text{B}(\text{OH})_4^-$ ; Branson, 2018). Incorporation of these elements can be impacted by environmental conditions (Gaetani and Cohen, 2006), physiological parameters (Sinclair, 2005), or mechanisms associated with calcification (e.g. Chalk et al., 2021). It is, however, unclear how these processes are impacted by the available nutrient budget, and as a result of both this and the difficulty of reconstructing them, changing nutrient conditions are rarely considered when making reconstructions of past environments using coral skeletal composition. Here, for the first time, the E/Ca (Li/Ca, B/Ca, Mg/Ca, Sr/Ca, Li/Mg) and  $\delta^{11}\text{B}$  composition of skeletal carbonate of *Acropora polystoma* and *Porites lichen*, cultured under four treatments of normal, enriched, and/or depleted nitrogen (as nitrate  $[\text{NO}_3^-]$ ) and phosphorus (as phosphate  $[\text{PO}_4^{3-}]$ ) concentrations, were investigated to explore the effects of nutrient enrichment and deprivation on traditional geochemical proxies for both temperature and the coral internal carbonate system that underpin

much of the use of coral skeleton geochemistry in palaeoceanography.

## 2. Materials and Methods

### 2.1. Coral Culturing

Specimens (Fig. 1) were cultured in artificial seawater (Table S1) in a closed coral mesocosm at the Coral Reef Laboratory, National Oceanography Centre, Southampton (D'Angelo and Wiedenmann, 2012). Parent colonies of both *Acropora polystoma* and *Porites lichen* grown in replete, optimal, and balanced nitrate and phosphate (HNHP) conditions, were fragmented, mounted onto ceramic tiles using epoxy resin, then returned to the replete conditions for four weeks to recover. After this recovery period, four fragments were left in the replete HNHP tank as a control, and sets of four fragments were placed into three further treatment tanks maintained at distinct dissolved inorganic nitrogen and phosphorus concentrations. These comprised a low nitrate/low phosphate treatment (LNLP) that was depleted in both nutrients, and two treatments characterised by imbalanced nutrient conditions formulated to mimic anthropogenic enrichments of  $[\text{NO}_3^-]$  and  $[\text{PO}_4^{3-}]$  respectively: high nitrate with low phosphate (HNLP), and low nitrate with high phosphate (LNHP). Corals were kept in each treatment and monitored for 140 days. Once the experimental period had finished, coral fragments were transferred from the treatment tanks to sterile water for a period of three days prior to sampling. Further details of the culturing set up can be found in Rosset et al. (2015, 2017) and Buckingham et al. (2022).

Nitrate and phosphate concentrations in the experimental systems were determined regularly through colourimetric detection methods using a HACH DR900 Colourimeter (Hach, USA) described in detail in Rosset et al. (2017). The long-term nutrient regimes over the duration of the experiment were the same as described in Buckingham et al. (2022): for HNHP,  $[\text{NO}_3^-]$  was  $\sim 4.5 \mu\text{M}$  and  $[\text{PO}_4^{3-}]$  was  $\sim 0.6 \mu\text{M}$  (N:P  $\sim 8:1$ ); for HNLP,  $[\text{NO}_3^-]$  was  $\sim 73 \mu\text{M}$  and  $[\text{PO}_4^{3-}]$  was not detectable (method detection limit =  $0.21 \mu\text{M}$ ); for LNHP,  $[\text{NO}_3^-]$  was  $\sim 0.06 \mu\text{M}$  and  $[\text{PO}_4^{3-}]$  was  $\sim 5.7 \mu\text{M}$  (N:P  $\sim 0.01$ ); and for LNLP both  $[\text{NO}_3^-]$  and  $[\text{PO}_4^{3-}]$  were not detectable (Fig. 1). Although mean  $[\text{NO}_3^-]$  and  $[\text{PO}_4^{3-}]$  concentrations of  $\sim 0.25 \pm 0.28 \mu\text{M}$  and  $\sim 0.13 \pm 0.08 \mu\text{M}$  respectively have been typically reported for coral reef waters (Kleypas et al., 1999), the high turnover rates of a dynamic nutrient budget (e.g. from reef fauna) means characterising the true nutrient availability through water measurements is extremely difficult (Furnas et al., 2005). Our LNLP treatment (as well as the nutrient imbalanced treatments) did not contain any fish or sponges that would make important contributions to this budget, and was characterised by  $[\text{NO}_3^-]$  and  $[\text{PO}_4^{3-}]$  below detection. It is therefore considered to be representative of nutrient starved conditions. The N and P concentrations of the HNHP condition fall within the range that characterises high nutrient reefs environments under the influence of upwelling or nutrient input from terrestrial environment (Szmant, 2002; Aston et al., 2019; Lapointe et al., 2019; Buckingham et al. 2022). Bearing in mind dynamic nutrient budgets exist on most reef systems, this treatment is most comparable to nutrient availability on coral reefs in nature (D'Angelo and Wiedenmann, 2014). Following that parent colonies of all corals in the present study were initially cultured in, and acclimated to, the HNHP treatment, corals grown under these nutrient conditions act as the control for our experiments. Our imbalanced nutrient conditions exceed typical seasonal variations (e.g. Lapointe et al., 2019), and therefore represent more extreme cases of anthropogenic  $[\text{NO}_3^-]$  and  $[\text{PO}_4^{3-}]$  enrichment, which will not necessarily follow seasonality.

Tanks were maintained at a constant temperature of  $\sim 26^\circ\text{C}$ , salinity of  $\sim 33.5 \text{ g/kg}$ , and pH of  $\sim 8.11$  (Table S1), with light intensities of  $\sim 110 \mu\text{mol m}^{-2} \text{ s}^{-1}$  as part of regular 12-hour light-dark cycles. Water pH was measured weekly using a Mettler Toledo EL20 pH probe. The pH of the four treatment tanks, converted to the total scale, varied slightly, with means ( $\pm 2\text{SD}$ ) of  $8.16 \pm 0.14$  for the HNHP treatment,  $8.13 \pm 0.19$

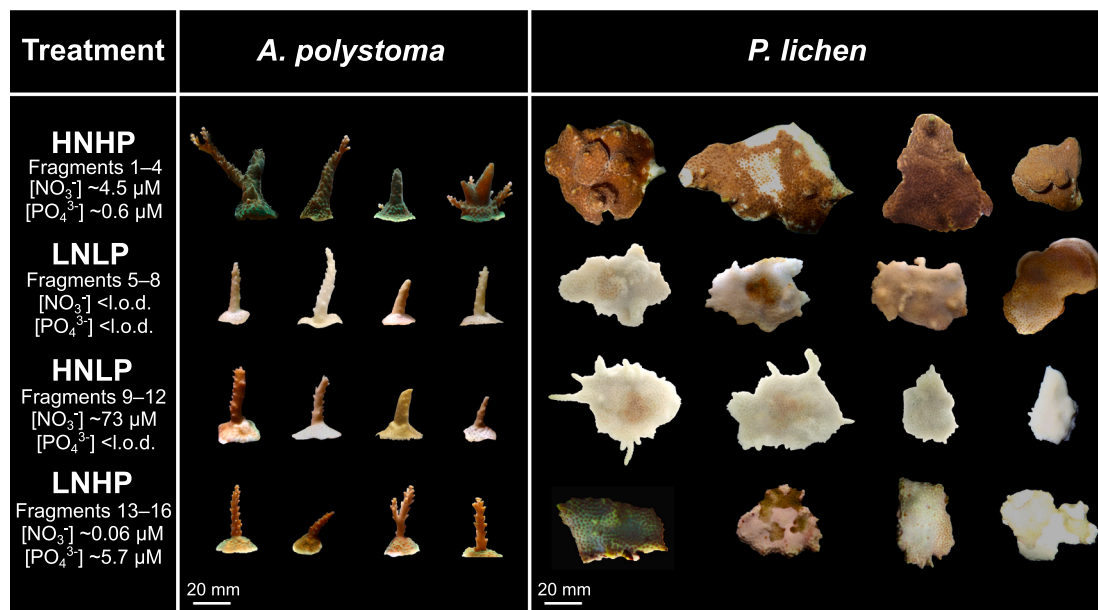


**Fig. 1.** *A. polystoma* and *P. lichen* specimens cultured under different nutrient treatments. Note bleaching on some samples due to nutrient stress, e.g. *A. polystoma* 6 and *P. lichen* 9–12, rather than temperature stress.

for the LNLP treatment,  $8.03 \pm 0.34$  for the LNHP treatment, and  $8.12 \pm 0.06$  for the HNLP treatment (Table S1). Temperature was measured daily with a glass thermometer, giving mean ( $\pm 2\text{SE}$ ) temperature readings of  $26.0 \pm 0.1$  °C for HNHP,  $25.9 \pm 0.1$  °C for LNLP,  $25.7 \pm 0.1$  °C for HNLP, and  $26.7 \pm 0.3$  °C for LNHP. Salinity of all treatments except LNHP was measured daily using a Hi-98319 Marine Waterproof Salinity Tester (Hanna Instruments Ltd., Leighton Buzzard, UK), giving mean ( $\pm 2\text{SE}$ ) values of  $33.8 \pm 0.1$  g/kg for HNHP,  $34.2 \pm 0.1$  g/kg for LNLP, and  $33.0 \pm 0.1$  g/kg for HNLP. DIC and total alkalinity were measured at different times to pH using a VINTDTA 3C system (Marianda), with the DIC measured via coulometry (coulometer 5011; UIC), and the total alkalinity by closed-cell titration (Dickson et al., 2007). DIC values are  $1147.7 \mu\text{mol/kg}$  for HNHP,  $1776.4 \mu\text{mol/kg}$  for LNLP,  $1809.1 \mu\text{mol/kg}$  for HNLP, and  $1650.0 \mu\text{mol/kg}$  for LNHP. The precision is  $\pm 3.6 \mu\text{mol/kg}$  for TA (or  $\sim 0.2\%$ ) and  $\pm 2.2 \mu\text{mol kg}^{-1}$  for DIC (or  $\sim 0.1\%$ ). Together, these measurements were used to verify the measurements taken via the pH probe.

## 2.2. Skeletal Growth

Growth measurements were taken weekly on the cultured corals. Linear growth and encrusting growth of the branching coral *A. polystoma* was measured using callipers (precision of  $\pm 0.1$  mm). For the encrusting coral *P. lichen*, areal growth was quantified using digital photography and imaging software. Photographs of the corals with a scale placed next to them were taken from above using an Olympus TG-4 digital camera that was mounted at a defined distance, using identical camera settings. The visible surface area of the corals was calculated in arbitrary units (a.u.) from the digital images using Fiji/ImageJ V1.44.

## 2.3. Symbiont Density

Corals grown in each nutrient treatment were sub-sampled, and zooxanthellae were extracted from two fragments of each species to measure symbiont density. An airbrush loaded with sterile seawater was used to remove zooxanthellae from a  $\sim 2\text{--}4 \text{ cm}^2$  area of each coral fragment (the exact area sampled was determined by image analysis). Three replicate 15 ml aliquots were centrifuged at 3,000 rpm for 10 min for purification, resulting sample pellets were then washed in 15 ml of sterile seawater before being centrifuged for a second time. The

supernatant was removed, sample pellets were resuspended in 10 ml of seawater, then 5  $\mu\text{l}$  of each aliquot was transferred to a haemocytometer. Algal cells were then counted under a light microscope using  $10\times$  magnification.

## 2.4. Photosynthetic Efficiency

A submersible pulse amplitude modulated (PAM) fluorometer was used to assess the weekly fluorescence-based maximum yield of photosystem II (Fv/Fm) in coral zooxanthellae over a period of 15 weeks. A Walz diving PAM (Heinz Walz GmbH, Effeltrich Germany), alongside accompanying WinControl V2.08 software, were used to measure and record Fv/Fm after eleven hours of acclimation to the daily dark period. The probe was held perpendicular to coral skeleton at a distance of 10 mm. Three repeat measurements were taken on each sample.

## 2.5. Coral Sampling

*A. polystoma* and *P. lichen* specimens (Fig. 1) were cleaned in a solution of 10%  $\text{H}_2\text{O}_2$  and 1.0 M  $\text{NH}_3$  for two days, before being ultrasonicated in  $18.2 \text{ M}\Omega \text{ cm}$  (ultrapure) water for 10 min and left to dry in a flow box. Specimens were then sectioned using a HC sintered diamond rotating saw and sampled using a scalpel; encrusting growth for *A. polystoma* and areal growth for *P. lichen*. The fragments,  $\sim 5 \text{ mm}^2$  in size, were then mounted in MetPrep EpoFLO high-purity epoxy resin, the coral surfaces were exposed using a HC sintered diamond rotating grinder, then samples were polished to reveal a flat and smooth surface using Kemet PSU-M polishing cloths with diamond in oil suspension (grades 15  $\mu\text{m}$ , 9  $\mu\text{m}$ , 3  $\mu\text{m}$ ). A final polish was performed using a 0.3  $\mu\text{m}$  grade polishing cloth and ultrawater, then samples were cleaned with alcohol in an ultrasonic bath. Prior to analysis by laser ablation (LA) inductively coupled plasma mass spectrometry (ICP-MS) and multi-collector inductively coupled plasma mass spectrometry (MC-ICP-MS), samples were ultrasonicated in ultrapure water for 5 min.

## 2.6. Solution ICP-MS

All geochemical analyses were performed at the geochemistry laboratory, School of Ocean and Earth Sciences, University of Southampton. Water samples were diluted by 134-times in 3% distilled  $\text{HNO}_3$

containing Be (20 ppb), In (5 ppb) and Re (5 ppb) for internal standardisation. Element concentrations of Li, B, Mg, Ca, and Sr were determined on a Thermo Scientific X-Series II Quadrupole ICP mass spectrometer (Thermo Fisher Scientific, Waltham, MA, USA). Accuracy was determined based on repeat analyses of Mediterranean Sea water standard (IAEA-B1) and are  $<5\%$  for Li/Ca, B/Ca, Mg/Ca and Sr/Ca and  $<10\%$  for Ba/Ca at  $2\sigma$ .

## 2.7. Solution MC-ICP-MS

Solution  $\delta^{11}\text{B}$  analysis on the culture waters were performed using a Thermo Scientific Neptune MC-ICP mass spectrometer following previously published procedures (Foster, 2008; Foster et al., 2013). Boron was isolated from the sample matrix by ion-exchange chromatography using 20  $\mu\text{l}$  Teflon columns containing Amberlite IRA743 resin. Mass bias corrections were applied by sample-standard bracketing using boron isotope standard NIST SRM951. Solution concentrations ranged from 40 to 50 ppb B and uncertainty ( $2\sigma$ ) ranges from  $\pm 0.2$ – $0.25\%$ , respectively, calculated from long term reproducibility of analyses of JCp-1, a *Porites* sp. coral standard (Inoue et al. 2004). Repeat analyses ( $n = 4$ ) of 50 ppb Mediterranean Sea water standard (IAEA-B1), which has the same matrix as our culture medium and was processed in the same way, returned a mean ( $\pm 2\text{SD}$ ) of  $39.7 \pm 0.15\%$ .

## 2.8. Laser Ablation ICP-MS

Elemental analysis of *A. polystoma* and *P. lichen* was performed on a Thermo Scientific X-Series II Quadrupole ICP mass spectrometer coupled to an Elemental Scientific Lasers (Bozeman, MT, USA) NWR193 excimer laser ablation system with a TwoVol2 ablation chamber. Samples were analysed for  $^{7}\text{Li}$ ,  $^{11}\text{B}$ ,  $^{24}\text{Mg}$ ,  $^{43}\text{Ca}$ , and  $^{86}\text{Sr}$  to enable calculation of E/Ca ratios. On-peak blank corrections were applied based on the mean intensities of preceding and succeeding blank measurement. Instrumental drift and mass bias were corrected by standard-sample bracketing to glass reference material NIST SRM612 and the values of Jochum et al. (2011). Samples and standards were ablated in line-mode, with each sample ablated once along the same track as used for the  $\delta^{11}\text{B}$  analyses (two ablation passes of a 1 mm line). Each analysis consisted of 1200 integration cycles of 0.173 s. Operating conditions are detailed in Table 1.

JCp-1 reference material and PS69/318-1, a cold water calcitic scleractinian octocoral (an in-house reference material), were ablated throughout the analytical session as a guide to internal precision, external reproducibility, and accuracy (Table 2). Internal precision, expressed as 2SE of the mean of 1200 integration cycles, was  $\leq 10\%$  for all ratios except Li/Ca, which was  $\leq 20\%$ . External reproducibility, expressed as 2SD of the mean of 6 analyses, was  $\leq 11\%$  for all ratios except Li/Ca, which was  $\leq 20\%$ . Mean accuracy of all ratios is to within 12% relative to published values: Foster et al. (2013) for PS69/318-1 and the interlaboratory comparison study by Hathorne et al. (2013) for JCp-1.

The sample E/Ca are presented after the data have been normalised to typical seawater compositions of 2.52  $\mu\text{mol/mol}$  Li/Ca, 42.07  $\mu\text{mol/mol}$  B/Ca, 5.14 mmol/mol Mg/Ca, and 8.82 mmol/mol Sr/Ca based on concentrations published by Li (1991) for Li, Lee et al. (2010) for B, and Millero et al. (2008) for Mg, Ca and Sr, using the following equation:

$$E/\text{Ca}_n = \frac{(E/\text{Ca})_m \times (E/\text{Ca})_{\text{cw}}}{(E/\text{Ca})_{\text{sw}}} \quad (1)$$

where  $n$  = normalised ratio of the coral,  $m$  = measured ratio of the coral,  $\text{cw}$  = culture water composition, and  $\text{sw}$  = seawater composition. Measured ratios are presented in the SI.

**Table 1**

Typical operating conditions for laser ablation ICP-MS analysis.

	$\delta^{11}\text{B}$ isotope analysis	Elemental analysis
<b>Instrument</b>		
Mass Spectrometer	Thermo Scientific Neptune Plus multi-collector inductively coupled plasma mass spectrometer	Thermo Scientific Quadrupole X-Series inductively coupled plasma mass spectrometer
Laser Ablation System	Elemental Scientific Lasers NWR193 excimer laser ablation system with a TwoVol2 ablation chamber	Elemental Scientific Lasers NWR193 excimer laser ablation system with a TwoVol2 ablation chamber
RF Power	1400 W	1200 W
Cones	Nickel skimmer (X) and jet sample	Standard nickel sample cone and XT skimmer
<b>Gas Flows</b>		
Cooling Gas (argon)	16 l min <sup>-1</sup>	13 l min <sup>-1</sup>
Auxiliary Gas (argon)	0.7 l min <sup>-1</sup>	0.8 l min <sup>-1</sup>
Make-up gas (argon)	1.0 l min <sup>-1</sup>	0.88 l min <sup>-1</sup>
Ablation cell carrier gas (helium)	1.0 l min <sup>-1</sup>	0.7 l min <sup>-1</sup>
Additional Gas (nitrogen)	0.006 l min <sup>-1</sup>	0.01 l min <sup>-1</sup>
<b>Ablation Conditions</b>		
Laser power density	$\sim 7.5$ – $8.0 \text{ J cm}^{-2}$	$\sim 7.5$ – $8.0 \text{ J cm}^{-2}$
Laser repetition rate	12 Hz	10 Hz
Laser beam size	50 $\mu\text{m}$ diameter	50 $\mu\text{m}$ diameter
Laser tracking speed	10 $\mu\text{m s}^{-1}$	10 $\mu\text{m s}^{-1}$
Ablation mode	Line	Line

## 2.9. Laser Ablation MC-ICP-MS

Boron isotope analysis of *A. polystoma* and *P. lichen* was performed on a Thermo Scientific Neptune Plus MC-ICP mass spectrometer coupled to an Elemental Scientific Lasers NWR193 excimer laser ablation system with a TwoVol2 ablation chamber. Analytical protocols broadly followed Standish et al. (2019).  $^{10}\text{B}$  and  $^{11}\text{B}$  were measured on the L3 and H3 Faraday cups respectively, both of which were installed with  $10^{13} \Omega$  resistors. Samples and standards were ablated to remove any surface contamination prior to data collection. Data were collected in static mode, with each analysis consisting of 100 integration cycles of 2.194 s. Dynamic blank corrections were applied cycle by cycle assuming a linear relationship between the preceding and succeeding blank measurements, instrumental mass bias was corrected by sample-standard bracketing with NIST SRM610 glass reference material and the isotope composition published by le Roux et al. (2004) and Standish et al. (2019), and matrix interferences from scattered Ca ions were corrected for based on a relationship between  $\delta^{11}\text{B}$  inaccuracy and  $^{11}\text{B}/\text{Ca}_{\text{interference}}$  for pressed pellets of carbonate reference materials JCt-1, *Tridacna gigas*, and JCp-1, *Porites* sp. coral (Inoue et al. 2004; Gutjahr et al., 2020), where the  $\text{Ca}_{\text{interference}}$  was measured at  $m/z$  of 10.10 using the L2 Faraday cup (installed with a  $10^{12} \Omega$  resistor). Samples and standards were ablated in line-mode (two passes over a length of 1 mm), with each sample ablated once. Data were screened and cycles falling outside of 2SD of the mean were removed. Operating conditions are detailed in Table 1. Internal reference material PS69/318-1 was ablated throughout the analytical session as a guide to internal precision, external reproducibility and accuracy (Table 2). Internal precision, expressed as 2SE of the mean of the 100 integration cycles, was  $\leq 0.4\text{\textperthousand}$ . The mean  $\delta^{11}\text{B}$  of the repeat analysis ( $n = 8$ ) was  $13.78 \pm 0.42\text{\textperthousand}$  (2SD), consistent with a solution measurement of  $13.83 \pm 0.29\text{\textperthousand}$  ( $2\sigma$ ) (Standish et al., 2019).

**Table 2**

LA-MC-ICP-MS and LA-ICP-MS analyses of reference materials JCp-1 and deep sea coral PS69/318–1. Uncertainties are  $\pm 2\text{SD}$  of repeats analyses. For  $\delta^{11}\text{B}$  analysis  $n = 8$ , and for E/Ca analysis  $n = 6$ .

	$\delta^{11}\text{B}$ (‰)	Li/Ca (µmol/mol)	B/Ca (µmol/mol)	Mg/Ca (mmol/mol)	Sr/Ca (mmol/mol)
PS69/318–1	$13.78 \pm 0.42$	$39.0 \pm 3.9$	$221.7 \pm 7.0$	$90.3 \pm 2.1$	$2.87 \pm 0.05$
JCp-1	–	$6.1 \pm 0.8$	$425.1 \pm 46.9$	$4.4 \pm 0.3$	$9.19 \pm 0.35$

The  $\delta^{11}\text{B}$  composition of the coral samples are presented in Table S2. However, in order to compare between treatments, the subtle  $\delta^{11}\text{B}$  differences of the culture water, which varied from  $-2.4$  to  $+1.3\text{‰}$  (Table S1), need to be accounted for. Boron isotope data are therefore discussed after normalisation to the isotopic composition of seawater  $\delta^{11}\text{B}_n$ :

$$\delta^{11}\text{B}_n = \left( \left( \frac{\delta^{11}\text{B}/^{10}\text{B}_{\text{sw}}}{\left( \left( \delta^{11}\text{B}/^{10}\text{B}_{\text{cw}} \right) / \left( \delta^{11}\text{B}/^{10}\text{B}_m \right) \right)} \right) \div \delta^{11}\text{B} / ^{10}\text{B}_{\text{NIST951}} - 1 \right) \times 1000 \quad (2)$$

where  $\delta^{11}\text{B}/^{10}\text{B}_{\text{sw}}$  is  $4.2038$  (Foster et al., 2010), and  $\delta^{11}\text{B}/^{10}\text{B}_{\text{NIST951}}$  is  $4.04367$  (Catanzaro et al., 1970). In order to investigate the response of internal pH to nutrient change, whilst also accounting for variations in the pH of the culture waters,  $\text{pH}_{\text{cf}}$  is calculated following Zeebe and Wolf-Gladrow (2001):

$$\text{pH}_{\text{cf}} = \text{pK}_B - \log \left( - \frac{\delta^{11}\text{B}_{\text{cw}} - \delta^{11}\text{B}_m}{\delta^{11}\text{B}_{\text{cw}} - \alpha_B \times \delta^{11}\text{B}_m - 1000 \times (\alpha_B - 1)} \right) \quad (3)$$

where  $\delta^{11}\text{B}_{\text{cw}}$  is the isotopic composition of the culture water for the respective treatment tank (see Table S1),  $\text{pK}_B$  (Dickson, 1990) is calculated individually for each treatment tank based on the measured temperature and salinity (Table S1), and the isotopic fractionation factor ( $\alpha_B$ ) =  $1.0272$  (Klochko et al. 2006). Finally,  $\Delta\text{pH}$  was calculated for each sample, where:

$$\Delta\text{pH} = \text{pH}_{\text{cf}} - \text{pH}_{\text{cw}} \quad (4)$$

## 2.10. Calculation of the Carbonate Chemistry

In order to investigate the effect of changes in nutrients on the carbonate chemistry of corals, carbonate ion  $[\text{CO}_3^{2-}]_{\text{cf}}$  (in  $\mu\text{mol/kg}$ ) has also been calculated for each sample following Chalk et al. (2021) using a simplified relationship between  $[\text{CO}_3^{2-}]_{\text{cf}}$ , borate ion  $([\text{B}(\text{OH})_4^-]_{\text{cf}}$  in  $\mu\text{mol/kg}$ ), and  $(\text{B/Ca})_m$  ( $\mu\text{mol/mol}$ ) fitted to the data of Holcomb et al. (2016):

$$[\text{CO}_3^{2-}]_{\text{cf}} = 0.00297 \times \left( \frac{[\text{B}(\text{OH})_4^-]_{\text{cf}}}{\text{B/Ca}_m} \times 10^6 \right) \quad (5)$$

where  $\text{B/Ca}$  is in  $\mu\text{mol/mol}$  and  $[\text{B}(\text{OH})_4^-]_{\text{cf}}$  (in  $\mu\text{mol/kg}$ ) is calculated following Dickson (1990) but using the respective, measured, culture water boron concentrations ( $[\text{B}]_{\text{cw}}$ ):

$$[\text{B}(\text{OH})_4^-]_{\text{cf}} = \frac{[\text{B}]_{\text{cw}}}{1 + [\text{H}]^+ / \text{K}_B} \quad (6)$$

$\Delta[\text{CO}_3^{2-}]$  was calculated using the following equation:

$$\Delta[\text{CO}_3^{2-}] = [\text{CO}_3^{2-}]_{\text{cf}} - [\text{CO}_3^{2-}]_{\text{cw}} \quad (7)$$

Dissolved inorganic carbonate [DIC] of the calcifying fluid (in  $\mu\text{mol/kg}$ ) was calculated from the  $\text{pH}_{\text{cf}}$ ,  $[\text{CO}_3^{2-}]_{\text{cf}}$ , and mean measured water salinities (g/kg) and temperatures (°C) in R for both the coral calcification fluid and the culture waters using the seacarb package v.3.3.0 (Gattuso et al., 2021).

$\Delta[\text{DIC}]$  is calculated using the following equation:

$$\Delta[\text{DIC}] = [\text{DIC}]_{\text{cf}} - [\text{DIC}]_{\text{cw}} \quad (8)$$

## 2.11. Statistical Treatment

Physiological and geochemical data were statistically compared to demonstrate whether differences between the replete HNHP treatment and the respective nutrient imbalanced (LNHP and HNLP) and deplete (LNLP) treatments were significant. Following a Shapiro-Wilks test which indicated that the data are, for the most part, normally distributed, t-tests were then applied. Results of the t-tests are presented in Table S3.

## 3. Results

### 3.1. Coral Growth

Corals cultured under all four nutrient treatments increased in size during the experimental period, albeit the degree of growth varied between treatments (Fig. 2 and Table S4). With respect to *A. polystoma* cultured in the replete HNHP treatment, mean ( $\pm 1\text{SD}$ ) linear growth was  $13.3 \pm 5.4$  mm and mean ( $\pm 1\text{SD}$ ) encrusting growth was  $7.3 \pm 1.6$  mm. Linear growth was significantly lower ( $p < 0.05$ , t-test, see Table S3) when corals were grown under the deplete or imbalanced conditions. In contrast, encrusting growth was significantly higher ( $p < 0.05$ , t-test) when corals were grown under HNLP conditions compared to those from the HNHP nutrient environment. Mean areal growth of *P. lichen* cultured in the HNHP treatment was  $3.6 \pm 1.3$  (a.u.). Relative to this, areal growth was significantly lower ( $p < 0.05$ , t-test) when grown under LNLP conditions.

### 3.2. Symbiont Density

The greatest symbiont densities were seen in the replete HNHP treatment for both species, with mean total cells per  $\text{mm}^2$  of  $11,858 \pm 512$  ( $\pm 2\text{SE}$ ) for *A. polystoma* and  $22,354 \pm 4,113$  for *P. lichen* (Fig. 3, Table S5). Relative to the nutrient replete conditions, densities were significantly lower ( $p < 0.05$ , t-test) in the deplete and imbalanced nutrient treatments in all cases: for *A. polystoma*, densities were 84% lower for LNLP, 83% lower for HNLP, and 66% lower for LNHP; for *P. lichen* densities were 94% lower for LNLP, 90% lower for HNLP, and 88% lower for LNHP.

### 3.3. Photosynthetic Efficiency

Fv/Fm measurements, used as a proxy for photosynthetic efficiency, remained stable for both species under HNHP (Fv/Fm of  $\sim 0.76$  for *A. polystoma* and  $\sim 0.62$  for *P. lichen*) and LNLP treatments (Fv/Fm of  $\sim 0.72$  for *A. polystoma* and  $\sim 0.62$  for *P. lichen*) (Fig. 4, Table S6). Under imbalanced nutrient conditions, photosynthetic efficiency of both *A. polystoma* and *P. lichen* decreased over time from starting values of  $\sim 0.6$ – $0.7$ ; linear regression  $p$ -values indicate slopes are significant at 95% confidence (Table S6). A Fv/Fm value  $< 0.5$ , as recorded at the end of the experimental period for *P. lichen* in the imbalanced nutrient treatments, is often used as an indicator of stress (Gorbunov et al., 2001). Yet strictly speaking, stress is inferred by the loss of photosynthetic efficiency over time, and this is recorded for both species in these imbalanced conditions.

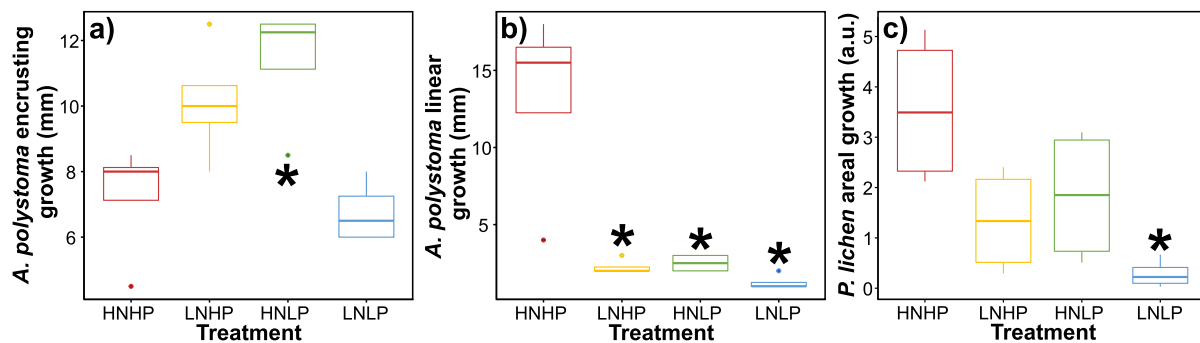


**Fig. 2.** Box plots showing skeletal growth of *A. polystoma* (a, b) and *P. lichen* (c) cultured under different nutrient treatments. Datasets different to their respective HNHP treatment at 95% confidence are marked with an asterisk.

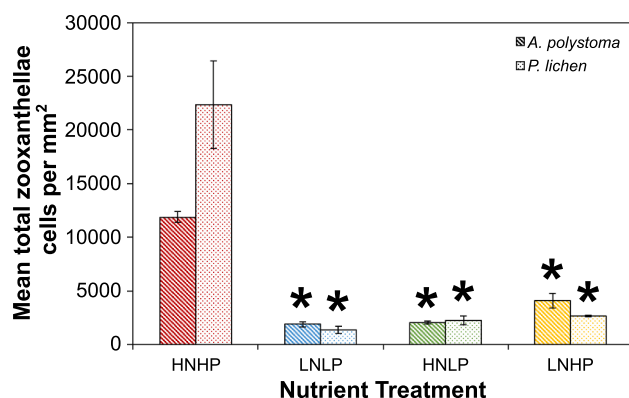


**Fig. 3.** Mean density of zooxanthellae ( $\pm 2\text{SE}$ ) on *A. polystoma* and *P. lichen* cultured under different nutrient treatments. Datasets different to their respective HNHP treatment at 95% confidence are marked with an asterisk.

#### 3.4. E/Ca Composition

For corals cultured in the nutrient replete (HNHP) treatment, mean ( $\pm 2\text{SE}$ ) E/Ca values are as follows: Li/Ca<sub>n</sub> of  $6.8 \pm 0.9 \mu\text{mol/mol}$  for *A. polystoma* and  $4.7 \pm 1.1 \mu\text{mol/mol}$  for *P. lichen*; B/Ca<sub>n</sub> of  $444.6 \pm 46.4 \mu\text{mol/mol}$  for *A. polystoma* and  $362.5 \pm 69.2 \mu\text{mol/mol}$  for *P. lichen*; Mg/Ca<sub>n</sub> of  $4.6 \pm 0.6 \text{ mmol/mol}$  for *A. polystoma* and  $3.6 \pm 1.0 \text{ mmol/mol}$  for *P. lichen*; Sr/Ca<sub>n</sub> of  $8.6 \pm 0.2 \text{ mmol/mol}$  for *A. polystoma* and  $8.0 \pm 0.2 \text{ mmol/mol}$  for *P. lichen*; Li/Mg<sub>n</sub> of  $1.5 \pm 0.2 \text{ mmol/mol}$  for *A. polystoma* and  $1.3 \pm 0.1 \text{ mmol/mol}$  for *P. lichen* (Table S2, Fig. 5).

Variability in E/Ca composition occurs as a function of culture medium nutrient content, with similar patterns recorded for both species (Fig. 5). Corals cultured under HNLP conditions are characterised by significantly lower Sr/Ca<sub>n</sub> ( $p < 0.05$ , *t*-test, see Table S3) compared to the HNHP nutrient environment. Li/Ca<sub>n</sub>, B/Ca<sub>n</sub>, and Mg/Ca<sub>n</sub>, are also significantly lower for *A. polystoma*, whilst Li/Mg<sub>n</sub> is significantly higher for *P. lichen*, cultured under HNLP conditions compared to the replete treatment. With respect to corals cultured under LNHP conditions, Sr/Ca<sub>n</sub> is significantly lower and Li/Mg<sub>n</sub> significantly higher ( $p < 0.05$ , *t*-test) compared to those cultured in the HNHP treatment. Li/Ca<sub>n</sub> and Mg/Ca<sub>n</sub> of *A. polystoma* are also significantly lower compared to those cultured in the HNHP treatment. Corals grown under nutrient deplete (LNLP) conditions are characterised by significantly lower B/Ca<sub>n</sub> and Sr/Ca<sub>n</sub> ( $p < 0.05$ , *t*-test, see Table S3) compared to the HNHP nutrient environment. Mg/Ca<sub>n</sub> is also significantly lower for *A. polystoma*, and Li/Mg<sub>n</sub> is significantly higher for *P. lichen*, cultured under LNLP conditions compared to the HNHP nutrient environment.

Correlations are strongest between Mg/Ca<sub>n</sub>, Sr/Ca<sub>n</sub>, and Li/Mg<sub>n</sub> for *A. polystoma*, all of which have Pearson correlation coefficients (*r*) of 0.65–0.86. Correlations between these ratios and Li/Ca<sub>n</sub> give an *r* of 0.43–0.81, whilst correlations are weakest when involving B/Ca<sub>n</sub> (*r* =

0.14–0.44). Similarly, correlations for *P. lichen* are strongest between Li/Mg<sub>n</sub> and Sr/Ca<sub>n</sub> (*r* = 0.69) and Mg/Ca<sub>n</sub> (*r* = 0.67), and are weakest when involving B/Ca<sub>n</sub> (*r* = 0.10–0.29) (Table 3, Figs. S1 and S2).

#### 3.5. Boron Isotope Ratio Composition and Carbonate Chemistry

*P. lichen* grown in the replete, HNHP, treatment yield a mean ( $\pm 2\text{SE}$ )  $\delta^{11}\text{B}_n$  of  $24.6 \pm 2.2\text{\textperthousand}$ , whilst *A. polystoma* grown in the HNHP treatment gave a mean ( $\pm 2\text{SE}$ )  $\delta^{11}\text{B}_n$  of  $25.6 \pm 1.3\text{\textperthousand}$  (Fig. 5, Table S2). Compared to the respective nutrient replete samples, corals grown in the imbalanced nutrient treatment LNHP are characterised by similar mean  $\delta^{11}\text{B}_n$  ( $23.9 \pm 1.0\text{\textperthousand}$  for *P. lichen* and  $25.6 \pm 0.8\text{\textperthousand}$  for *A. polystoma*). Corals grown in both the imbalanced nutrient treatment HNLP and the deplete nutrient treatment LNLP are characterised by similar, or slightly higher, mean  $\delta^{11}\text{B}_n$ :  $24.9 \pm 1.3\text{\textperthousand}$  for *P. lichen* and  $26.5 \pm 0.4\text{\textperthousand}$  for *A. polystoma* for the former, and  $24.0 \pm 2.0\text{\textperthousand}$  for *P. lichen* and  $26.3 \pm 0.4\text{\textperthousand}$  for *A. polystoma* for the latter. No treatments are different at a 95% confidence level based on the *t*-tests (Table S3). Overall, the range in  $\delta^{11}\text{B}$  due to varying nutrient concentration was  $\sim 1\text{\textperthousand}$ . Boron geochemistry is an effective tracer of the coral carbonate system, permitting calculation of pH,  $[\text{CO}_3^{2-}]$  and [DIC] (e.g. McCulloch et al., 2017), all of which are estimated here. Since the subtle variations in culture media pH may obscure relationships in  $\delta^{11}\text{B}$ -space, it is more informative to compare between the treatments in terms of  $\Delta\text{pH}$  (Equation (4)). Corals grown in the replete HNHP treatment are characterised by  $\Delta\text{pH}$  ( $\pm 2\text{SE}$ ) of  $0.43 \pm 0.08$  for *A. polystoma* and  $0.37 \pm 0.14$  for *P. lichen* (Fig. 6, Table S2). Corals cultured in imbalanced nutrient treatments HNLP and LNHP are characterised by relatively larger  $\Delta\text{pH}$  (Fig. 6, Table S2), and for *A. polystoma* these differences are significant ( $p < 0.05$ , *t*-test, see Table S3). The  $\Delta\text{pH}$  of corals cultured under LNLP conditions was not significantly different to those from the HNHP nutrient environment at 95% confidence.

The mean  $\Delta[\text{CO}_3^{2-}]$  ( $\pm 2\text{SE}$ ) of HNHP samples are  $1,024 \pm 62 \mu\text{mol/kg}$  for *P. lichen* and  $884 \pm 89 \mu\text{mol/kg}$  for *A. polystoma* (Fig. 6, Table S2). Mean  $\Delta[\text{CO}_3^{2-}]$  was significantly higher ( $p < 0.05$ , *t*-test, see Table S3) for both species of corals when specimens were cultured under the LNHP conditions, and significantly lower for *A. polystoma* when cultured under LNLP conditions. The mean  $\Delta[\text{DIC}]$  ( $\pm 2\text{SE}$ ) of HNHP samples are  $3,144 \pm 1,118 \mu\text{mol/kg}$  for *P. lichen* and  $2,187 \pm 443 \mu\text{mol/kg}$  for *A. polystoma* (Fig. 6, Table S2). Mean  $\Delta[\text{DIC}]$  was significantly lower ( $p < 0.05$ , *t*-test) for *A. polystoma* cultured under LNHP conditions.

## 4. Discussion

### 4.1. The effect of nutrient enrichment and depletion on coral physiology

Corals cultured in replete HNHP conditions (nitrate of  $\sim 4.5 \mu\text{M}$ , phosphate of  $\sim 0.6 \mu\text{M}$ ) were characterised by stable photosynthetic efficiencies and the greatest symbiotic densities. Net skeletal growth of *A. polystoma* (i.e. linear growth plus encrusting growth) was also

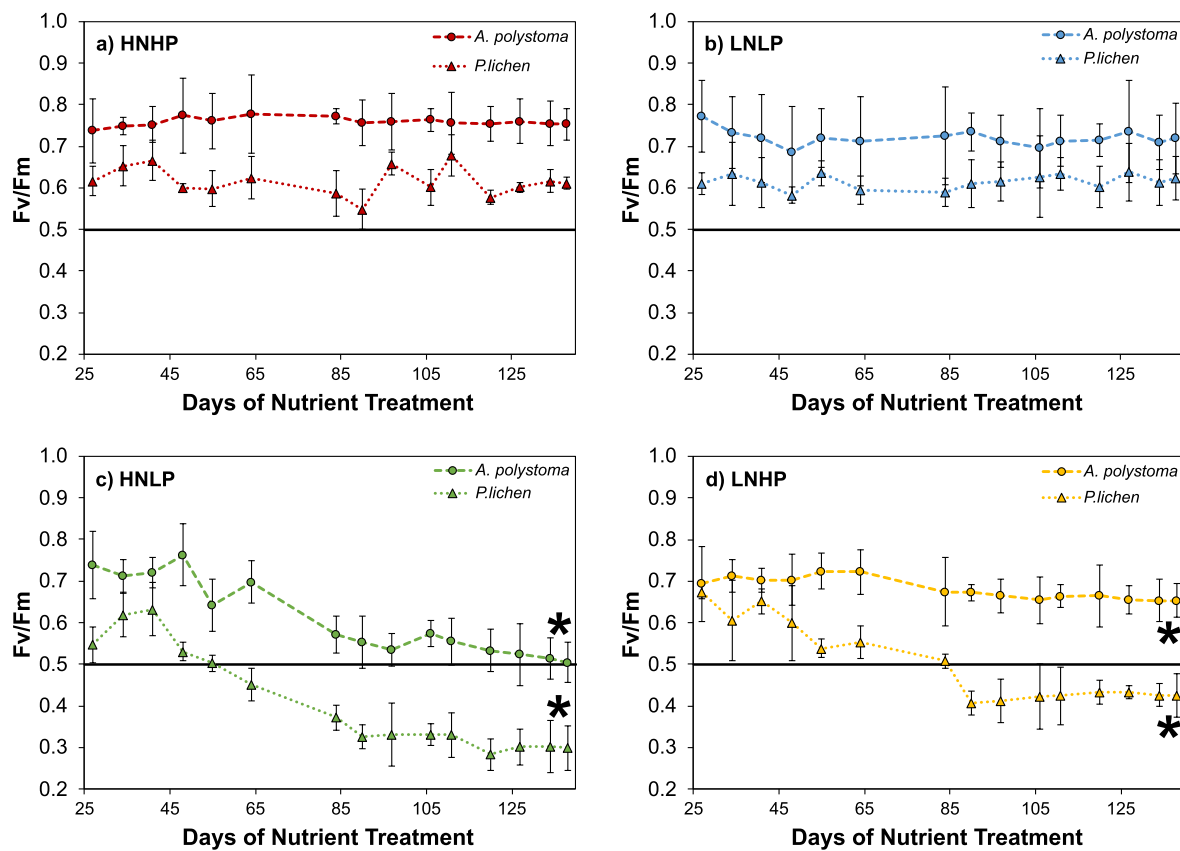


**Fig. 4.** Photosynthetic efficiency of coral zooxanthellae on *A. polystoma* and *P. lichen* cultured under different nutrient treatments over a period of 15 weeks. Uncertainties are 2SE of the three replicate measurements. Data series marked with an asterisk slope at a confidence of 95%.

greatest in those grown in the replete treatment, with this being driven primarily by high linear growth (minimal encrusting growth was observed). Meanwhile, for *P. lichen*, samples grown in the replete treatment recorded the greatest degree of areal growth.

Symbiotic densities were significantly lower for corals cultured in the deplete nutrient treatment LNLP (both nitrate and phosphate at or below detection) compared to the replete treatment, results that are consistent with a study on *Euphyllia paradoxa* by Rosset et al. (2015), although it should be noted that these mean differences between treatments are no larger than those typically observed seasonally at single sites (Fagoonee et al., 1999; Costa et al., 2005). In both this study and Rosset et al. (2015), the photosynthetic efficiency was not impacted, with Rosset et al. (2017) hypothesising that normal photosynthetic efficiency can be explained because both N and P are both depleted and thus there is a reduced demand for phosphorus from non- or slow-growing algal populations (D'Angelo and Wiedenmann, 2014). Skeletal growth was impacted, with *A. polystoma* recording significantly lower linear growth (and net skeletal growth), and *P. lichen* recording significantly lower areal growth. This apparently contradicts the view that corals typically calcify faster when nutrients are scarce (McConaughey, 2012, and references therein). However, growth rates (measured either as linear extension or areal growth) do not necessarily mirror calcification rate. Furthermore, it can be difficult to compare studies that contrast corals cultured under different nutrient conditions; the LNLP treatment here is considered to be nutrient starved (i.e. stressed) where levels of nitrate and phosphate are at levels lower than typical reef environments.

The effect of nitrogen enrichment on coral calcification is dependent on its chemical form, concentration, coral species, and duration of enrichment, with biological mechanisms also playing a key role (Ferrier-Pagès et al., 2000). For example, additional nitrogen can be incorporated into algal biomass, resulting in a decrease in the transfer of photosynthetic products (e.g. C) from symbiont to coral and, as a

consequence, lower rates of coral calcification (Dubinsky et al. 1990; Stambler et al. 1991). There is also the potential for an increase in competition between algae and host for inorganic carbon (Stambler et al. 1991; Marubini and Davies 1996). Ferrier-Pagès et al. (2000) reported that the growth of *Stylophora pistillata* was dependent on nutrient concentrations, with a decrease reported at ammonium concentrations of 20  $\mu$ M. This was consistent with a decrease in skeletal growth of *Pocillopora damicornis* at similar ammonia concentrations (15  $\mu$ M) reported by Stambler et al. (1991), although Steven and Broadbent (1997) reported no decrease in growth of *Acropora palifera* at lower concentrations of 4  $\mu$ M. In contrast, nitrogen as nitrate at similarly low concentrations (1–20  $\mu$ M) has typically been reported to lead to a decrease in growth of a variety of coral species (Tomascik and Sander, 1985; Bell and Tomascik 1993; Marubini and Davies, 1996), with the exception of Dollar (1994) who reported no negative change in growth of *Porites rus* at (unmeasured) high nitrogen, and Atkinson et al. (1995) who recorded elevated growth for a wide variety of species in nitrate of up to 5  $\mu$ M (which was linked to high levels of CO<sub>2</sub>).

In this study, although we did not directly quantify calcification rates, linear growth of *A. polystoma* was significantly lower in HNLP treatments (nitrate of  $\sim$ 73  $\mu$ M) when compared to those grown in the replete treatment (nitrate of  $\sim$ 4.5  $\mu$ M), driving lower net skeletal growth. Whilst encrusting growth was significantly higher — indicating a shift in skeletal growth strategies — the overall decrease in net growth of *A. polystoma* during nitrogen enrichment is consistent with both the general picture, as well as previous work on this specific species; Buckingham et al. (2022) note that such nutrient conditions were typically associated with either no effect or decreases of both linear growth and calcification for *Acropora* spp. *P. lichen* cultured in the HNLP treatment in this study also show lower levels of skeletal growth compared to those cultured under replete HNHP conditions. Similarly, Ferrier-Pagès et al. (2000) reported a decrease in growth of *S. pistillata*

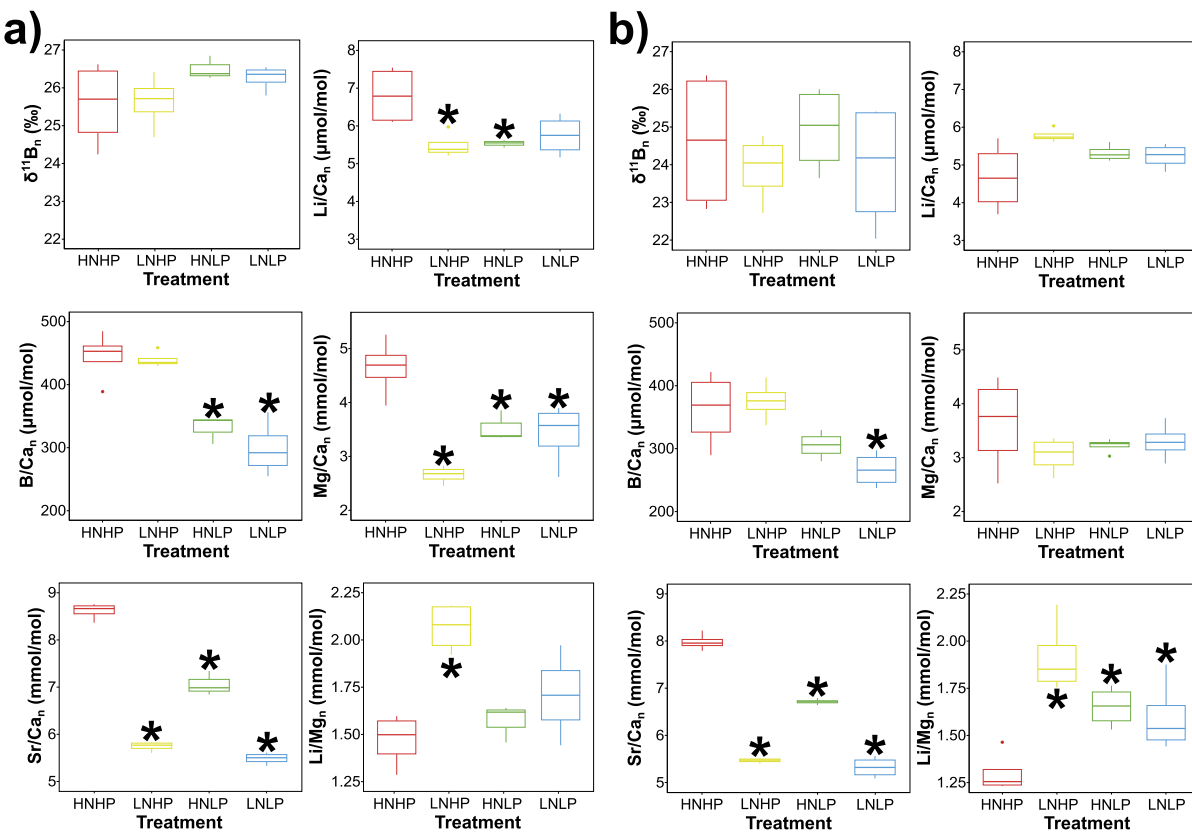


**Fig. 5.** Normalised  $\delta^{11}\text{B}$  and E/Ca composition of (a) *A. polystoma* (encrusting growth) and (b) *P. lichen* (areal growth) cultured under different nutrient treatments. Datasets different to their respective HNHP treatment at 95% confidence are marked with an asterisk.

**Table 3**

Pearson correlation coefficients between E/Ca ratios for *A. polystoma* (italic cells) and *P. lichen* (bold cells). Coefficients  $\geq 0.5$  are underlined.

Ratio	Li/Ca <sub>n</sub>	B/Ca <sub>n</sub>	Mg/Ca <sub>n</sub>	Sr/Ca <sub>n</sub>	Li/Mg <sub>n</sub>
Li/Ca <sub>n</sub>	–	0.34	<u>0.81</u>	0.68	0.43
B/Ca <sub>n</sub>	<b>0.22</b>	–	0.14	<u>0.44</u>	0.19
Mg/Ca <sub>n</sub>	<b>0.26</b>	<b>0.29</b>	–	<u>0.80</u>	<u>0.86</u>
Sr/Ca <sub>n</sub>	<u>0.50</u>	0.24	<u>0.40</u>	–	<u>0.65</u>
Li/Mg <sub>n</sub>	<u>0.53</u>	0.10	<u>0.67</u>	<u>0.69</u>	–

with phosphorus enrichment of 2  $\mu\text{M}$ . Results presented here from the imbalanced LNHP nutrient enrichment (phosphate of  $\sim 5.7 \mu\text{M}$ ) are consistent with this: lower areal growth is recorded in *P. lichen* and lower net growth is recorded for *A. polystoma*, driven by significantly lower linear growth (albeit alongside higher encrusting growth) compared to corals grown under nutrient replete conditions. McConaughey (2012) demonstrated that calcification is typically higher when nutrient levels are lower, suggesting a positive relationship between calcification-generated proton export and nutrient uptake. Accordingly, high nutrient availability may result in reduced calcification (McConaughey, 2012), a hypothesis that is consistent with the reduced growth recorded during the LNHP and HNLP treatments here. It has also been proposed that  $[\text{PO}_4^{3-}]$  can retard  $\text{CaCO}_3$  nucleation and precipitation rates (e.g. in foraminifera, Henehan et al., 2015), which offers a further mechanism for reduced growth in the LNHP treatment. However, as the imbalanced treatments are also starved of either nitrate or phosphate, this starvation could also be a key driver of the physiological responses recorded.

Symbiont densities for both species were significantly lower in the imbalanced treatments than the nutrient replete treatment (with these differences again being no larger than those recorded seasonally), and

their photosynthetic efficiencies decreased throughout the duration of the experiment. Fv/Fm values for *P. lichen* indicate that this species was experiencing stress. With respect to HNLP conditions, this is again consistent with the findings of Rosset et al. (2017) who showed that symbiosis was disturbed, and algal photosynthesis impacted, when *E. paradoxa* was cultured in phosphate limited but nitrate replete water. Indeed, Wiedenmann et al. (2013) had also previously demonstrated that phosphate starvation of zooxanthellae at high N:P can disturb the photosynthetic capacity of zooxanthellae through altering the normal ionic character of their photosynthetic membranes, making corals more susceptible to bleaching. A number of other studies found that nutrient enrichment led to an increase in the rate of maximal gross photosynthesis and zooxanthellae density on a range of coral species (Hoegh-Guldberg and Smith 1989; Dubinsky et al. 1990; Marubini and Davies 1996; Ferrier-Pagès et al. 2000). With respect to the findings of Ferrier-Pagès et al. (2000), this was compared to an unenriched nutrient treatment of  $<0.1 \mu\text{M}$  phosphorus and  $<0.5 \mu\text{M}$  nitrate, which is more akin to the LNLP treatment here and can therefore be deemed as being a consistent result. Nonetheless, Rosset et al. (2017) demonstrated that *E. paradoxa* can tolerate low nitrate conditions when phosphate is replete (LNHP) without negative effects, suggesting a better adaptation to nitrogen limitation for this species. This was not the case for the *A. polystoma* and *P. lichen* studied here, with both symbiotic densities and photosynthetic efficiency negatively impacted in both HNLP and LNHP treatments, further highlighting species-specific responses.

#### 4.2. The effect of nutrient enrichment and depletion on geochemical proxies

The nutrient treatments clearly impact coral physiology, and likewise the geochemical signature of *A. polystoma* and *P. lichen* skeleton also vary with nitrate and phosphate enrichment and depletion. With

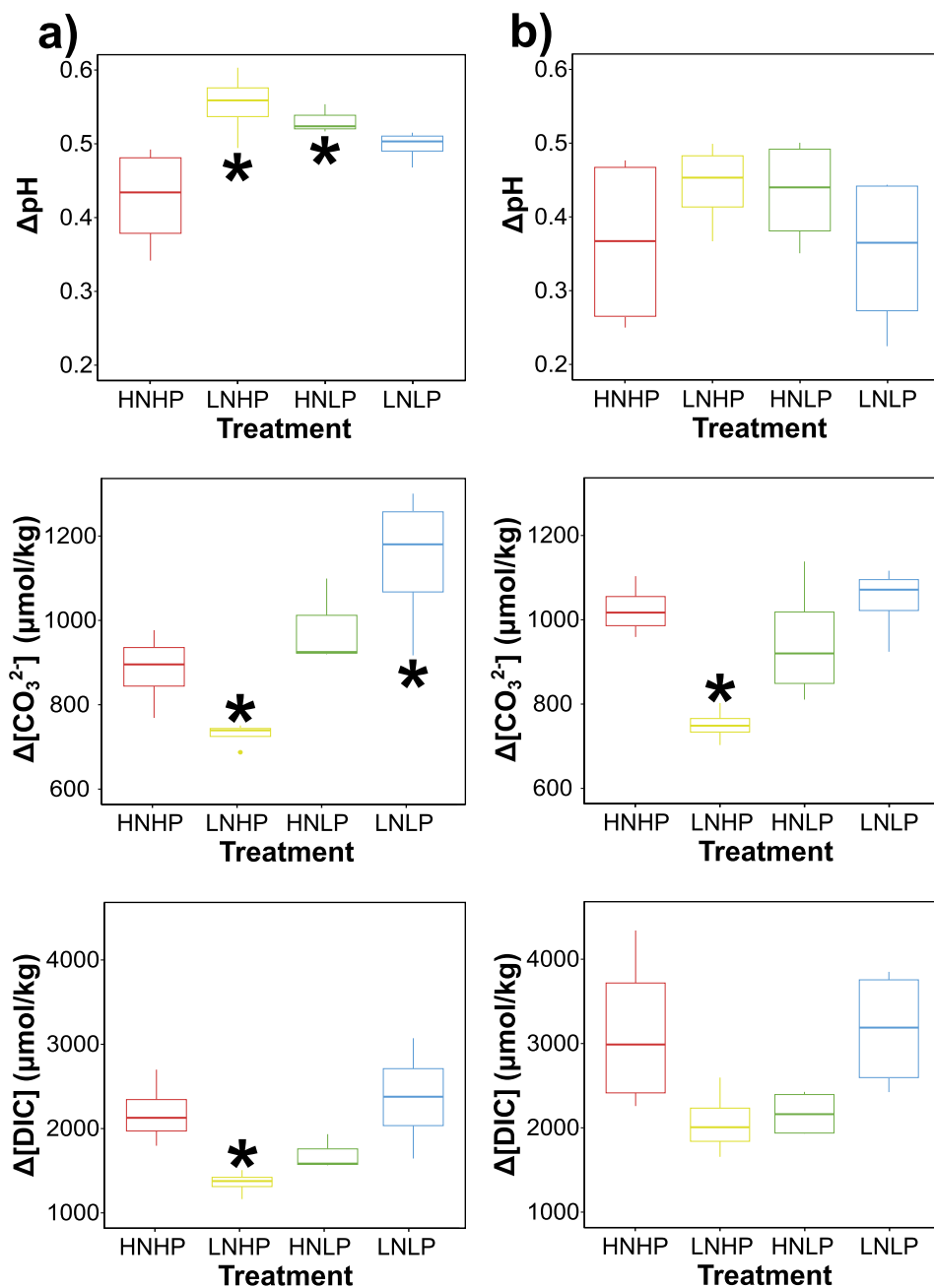


**Fig. 6.**  $\Delta\text{pH}$ ,  $\Delta[\text{CO}_3^{2-}]$ , and  $\Delta[\text{DIC}]$  of *A. polystoma* (a) and *P. lichen* (b) cultured under different nutrient treatments. Datasets different to their respective HNHP treatment at 95% confidence are marked with an asterisk.

respect to E/Ca, the two coral species show remarkably similar relationships between nutrient treatments. For example, after normalisation to culture water, Sr/Ca is lower and Li/Mg is higher (at 95% and 80% confidence levels respectively), in the deplete and imbalanced treatments for both species compared to their respective replete treatment (Fig. 5).

The Sr/Ca, Li/Mg, and Mg/Ca of scleractinian coral skeletons are all applied as seawater temperature proxies (Beck et al., 1992; Sinclair et al., 1998; Watanabe et al. 2001; Fallon et al., 2003; Montagna et al. 2014; Alpert et al. 2016). Ross et al. (2019) demonstrated that Sr/Ca of tropical (branching and foliose) coral skeletons changes by  $-0.06 \text{ mmol/mol } ^\circ\text{C}^{-1}$  (a figure consistent with a study by Corrège, 2006, for *Porites* spp.), whilst skeletal Li/Mg changes by approximately  $-0.08 \text{ } \mu\text{mol/mol } ^\circ\text{C}^{-1}$ . Based on these relationships, and the differences we find between the replete, imbalanced and depleted treatments, it is

apparent that the two temperature proxies have very different sensitivities to changes in nutrient levels (Fig. 7a). The Sr/Ca temperature proxy is particularly sensitive to changes in nutrient concentrations, exhibiting biases equivalent to  $+21$  to  $+52$   $^\circ\text{C}$  between treatments (x-axis, Fig. 7a and b). The low nitrate treatments are most affected and there is little difference between the two species studied. The Li/Mg temperature proxy is impacted to a small degree exhibiting changes equivalent to  $-2$  to  $-7$   $^\circ\text{C}$  and with no clear differences between species or treatment (y-axis, Fig. 7a). Based on a study of *Montastrea faveolata* by Watanabe et al. (2001), the Mg/Ca temperature proxy changes by  $0.28 \text{ mmol/mol } ^\circ\text{C}^{-1}$ . This proxy is therefore impacted to a similar degree as the Li/Mg, with changes equivalent to  $-1$  to  $-7$   $^\circ\text{C}$  (y-axis, Fig. 7b).

The observed responses in the E/Ca signature of the coral samples between nutrient treatments demonstrates that changing nutrient levels, and the impacts these have on coral physiology, significantly alters the

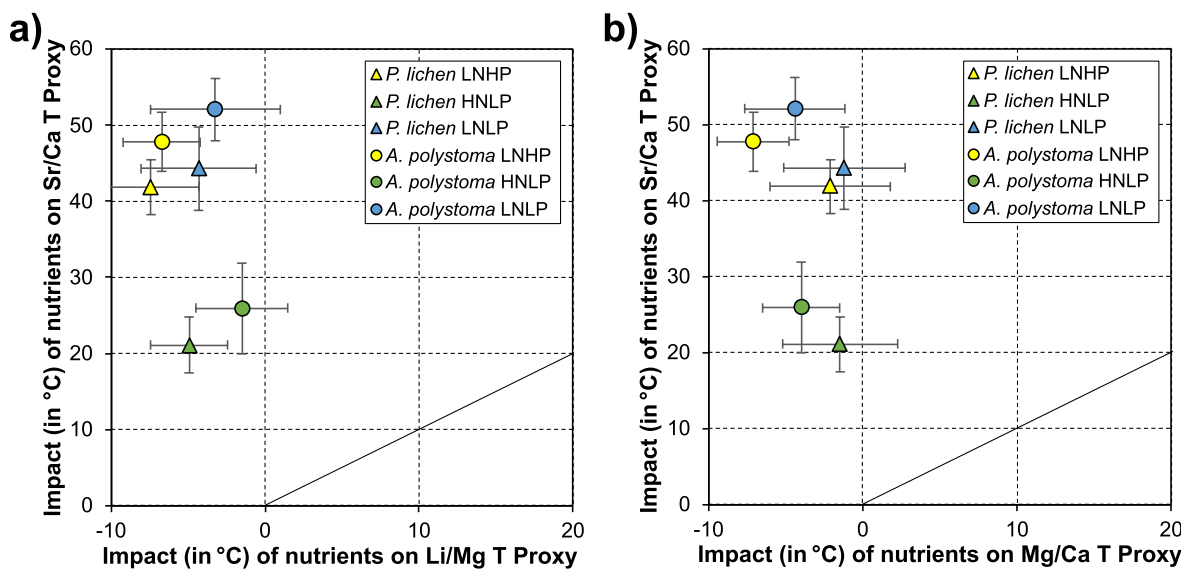


**Fig. 7.** Impact of dissolved nutrient levels to geochemical temperature proxies: (a) Sr/Ca proxy compared to Li/Mg proxy, (b) Sr/Ca proxy compared to Mg/Ca proxy. Solid black line represents 1:1 ratio.

geochemical signature of scleractinian corals. Ambient nutrient levels are not typically considered when calibrating and applying geochemical proxies in coral skeletons. Although the variations in nutrient levels here are extreme, our results suggest variable nutrients may play a hitherto under-appreciated role in site specific variations in coral E/Ca composition. This is especially so for Sr/Ca, which is reduced by around 30% between the nutrient replete and nutrient depleted treatments (Fig. 5). As we demonstrated in Fig. 7, this implies even small variations in nutrient concentration (or nutrient imbalance) could have dramatic consequences on reconstructed SST and could play an underappreciated role in driving 'site specific' Sr/Ca-SST calibrations (e.g. Alpert et al., 2016). Furthermore, given the differential sensitivities of the proxies, nutrient effects could be invoked as an explanation for when the Sr/Ca proxy diverges from that of Li/Mg or Mg/Ca. A possible avenue for future research is therefore to explore whether it is possible to correct temperature proxies for nutrient effects, or to deconvolve nutrient conditions from multiple elemental ratios.

The boron isotope-pH proxy is also widely used in palaeoenvironmental studies of corals (e.g. Wei et al., 2009; D'Olivo et al., 2019; Fowell et al., 2018), with a 1‰ difference in  $\delta^{11}\text{B}$  equating to an approximate change of 0.1 pH units. Due to the differing  $\delta^{11}\text{B}$  and pH of the culture water from each treatment, this will be discussed here in terms of  $\Delta\text{pH}$ , i.e. the difference between the  $\text{pH}_{\text{cf}}$  and  $\text{pH}_{\text{cw}}$  (Eq. (4)). Corals grown in the nutrient deplete or imbalanced treatments are up to 0.13 pH units higher than their respective replete treatments (Fig. 6). In *A. polystoma*, imbalanced treatments are different by 0.11 (HNLP) and 0.13 (LNHP) pH units, significant at 95% confidence, and the deplete treatment (LNLP) is different by 0.07 pH units, significant at 68% confidence. In *P. lichen*, the imbalanced treatments again show the largest difference relative to the replete treatment: ~0.07–0.08 pH units different, but only the LNLP is different at a significance of 68% confidence. The  $\Delta\text{pH}$  of the LNLP treatment is indistinguishable from the replete. As  $\delta^{11}\text{B}$ -pH changes by around 0.3–0.5 pH units per 1 unit of external pH change (McCulloch et al., 2012b), changes induced by nutrients are therefore considerable, and larger than the ~0.1 pH unit change in external seawater pH caused by anthropogenic acidification of the ocean (e.g. Fowell et al. 2018 and references therein). The impact from anthropogenically-induced nutrient disturbances should therefore also be considered when generating  $\delta^{11}\text{B}$ -based records of seawater pH, or assessing coral response to pH change, particularly given the increased occurrences of nutrient disturbance in tandem with increasing anthropogenic acidification and warming. Indeed, it may be that an

imbalance of nutrients could contribute to obscuring the  $\delta^{11}\text{B}$ -pH signals associated with ocean acidification, as is frequently observed (e.g. Fig. S1 from Fowell et al., 2018). It is also worth noting that this impact may not be equal amongst all species of coral, as based on the evidence presented here *P. lichen* appears less affected than *A. polystoma*.

It is therefore apparent that when geochemical proxies are being applied to reconstruct past environments, consideration must be paid to the evolution of nutrient budgets within a given study region. Particular care is needed when samples derive from regions where nutrient budgets have been disturbed by anthropogenic activity. One option is to use proxies for nutrient conditions, such as P/Ca (e.g. LaVigne et al., 2010), in conjunction with other proxies so these effects can be noted, minimised, normalised, or screened out. Alternatively, if independent proxies from the same parameter can be used in tandem, such as Sr/Ca and Li/Mg for SST studies (Cuny-Guiriec et al., 2019), their divergence could be used to identify when such impacts may be significant, or even to identify the occurrence of such nutrient enrichment/depletion events.

#### 4.3. The effect of nutrient enrichment and imbalance on calcification fluid composition

New coral skeleton is precipitated from semi-isolated pools of modified seawater located in a sub-micron sized space called the extracellular calcifying medium (ECM), sandwiched between the coral animal and its existing skeleton (Tambutté et al., 2007, 2012, Gagnon et al., 2012). Through the deployment of enzymatic pumps (e.g. Ca-ATPase: Ip et al., 1991) and the secretion of acid-rich proteins (Mass et al., 2013), the coral animal has a high degree of control on the carbonate system within these pools, enabling such modification (Ram and Erez, 2021). This enables elevation of parameters such as pH, DIC, and as a consequence aragonite saturation state ( $\Omega$ ), in order to favour crystal growth (e.g. Sevilgen et al., 2019).

As noted above,  $\Delta\text{pH}$  (the degree of pH elevation in the ECM) varies between the nutrient treatments (Fig. 6), with greater upregulation seen in the nutrient imbalanced treatments. Similarly, other aspects of the carbonate system in the calcifying fluid vary as a function of nutrient concentration: for both species,  $\Delta[\text{DIC}]$  is lowest in the imbalanced nutrient treatments and highest in the nutrient deplete treatment, whilst  $\Delta[\text{CO}_3^{2-}]$  is lowest in the imbalanced LNHP treatment and highest in the nutrient deplete treatment (Fig. 6). In particular,  $\Delta[\text{DIC}]$  is well-correlated with  $\Delta\text{pH}$  (Fig. 8).

Current models of calcium carbonate biomineralisation in coral

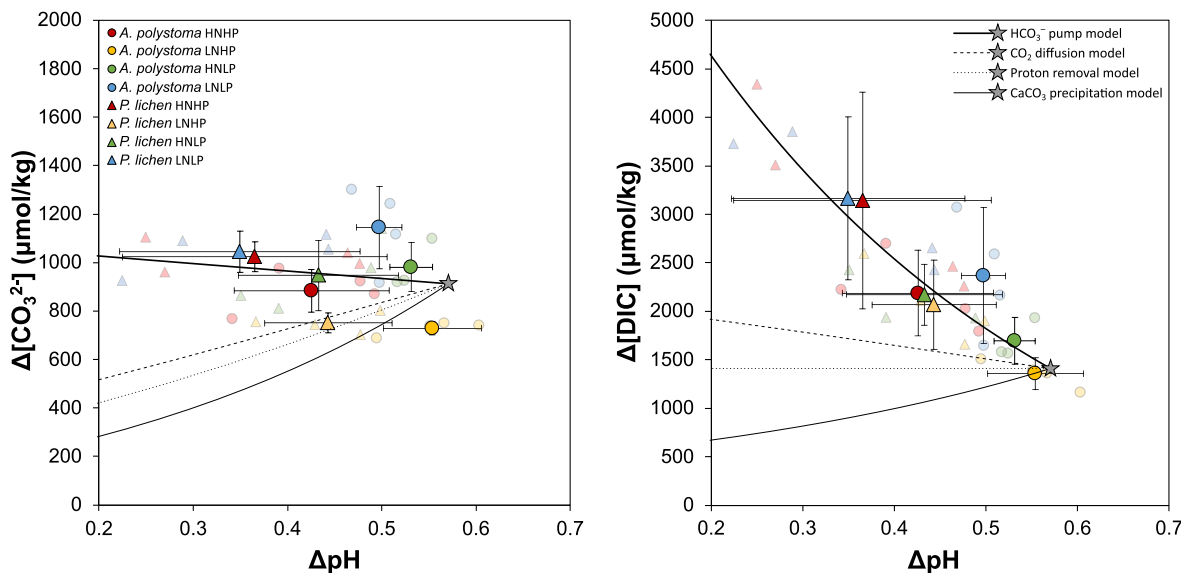


**Fig. 8.**  $\Delta[\text{CO}_3^{2-}]$  and  $\Delta[\text{DIC}]$  versus  $\Delta\text{pH}$  of *A. polystoma* and *P. lichen* cultured under different nutrient treatments. Uncertainties are 2SE of the mean of the repeat analyses. The trend lines shows the evolution of the carbonate fluid as: (i)  $\text{HCO}_3^-$  is added, simulated by increasing [DIC] and ALK in a 1:1 ratio, (ii) metabolic  $\text{CO}_2$  diffuses in, increasing [DIC] with alkalinity remaining constant, (iii) protons are removed by the CaATPase enzymatic pump, decreasing alkalinity with [DIC] remaining constant, and (iv) precipitation of  $\text{CaCO}_3$  that decreases alkalinity and [DIC] with 2:1 ratio.

favour a precursor phase of amorphous calcium carbonate (ACC; Mass et al., 2017). It has subsequently been proposed that this ACC, which forms in vesicles of intracellular calcifying fluid and is exocytosed into the ECM, attaches to the mineral growth front via particle attachment before voids are infilled through ion attachment processes (Sun et al., 2020; Gilbert et al., 2022). Whilst ACC formation and its particle attachment are clearly important, significant amounts of calcium carbonate is still deposited by later ion attachment processes, and previous studies have shown how simplified geochemical models can provide useful insights in coral biomineralisation (McCulloch et al., 2012a; Guo, 2019). Here, we therefore assume that ECM chemistry is important in driving the skeletal geochemistry, and assess the trends recorded in the cultured coral's carbonate chemistry with respect to such a simplified, closed system, geochemical model.

Based on the model presented by Guo (2019), the state of the carbonate system in the ECM is assumed to be determined by the balance between: (i) the degree of proton removal by the CaATPase enzymatic pump which increases  $\text{pH}_{\text{cf}}$  and does not directly influence fluid  $\text{DIC}_{\text{cf}}$ ; (ii) the degree of DIC-enrichment caused by either diffusion of  $\text{CO}_2$  or the active pumping of  $\text{HCO}_3^-$  by bicarbonate ion transporters (BAT; Zoccola et al., 2015), both of which cause pH to decline and calcification fluid DIC to increase; (iii) precipitation of  $\text{CaCO}_3$  that, by removing 2 M of alkalinity and 1 M of DIC per 1 M of  $\text{CaCO}_3$ , lowers both DIC and pH; and (iv) the admixture and modification of seawater into the calcifying space that drives the internal carbonate system back towards external seawater values. The trends shown in Fig. 8 are most easily explained by variations in the degree of DIC-enrichment of the calcifying space, such that for balanced nutrients (either replete or depleted) DIC-enrichment of the calcifying fluid is higher than for the imbalanced nutrients, with a tendency for the LNLP treatment to have the highest extent of DIC-enrichment. The evolution of the carbonate chemistry within the calcifying fluid as  $\text{HCO}_3^-$  is added can be simply modelled by increasing DIC and ALK in a 1:1 ratio. Plotted on Fig. 8, good consistency between the model and the calculated carbonate chemistry for the measured corals suggests that variable addition of  $\text{HCO}_3^-$  to the calcifying space can largely explain the variation recorded.

Disruption of the DIC transporting mechanism can occur in two ways: (i) the active transport of  $\text{HCO}_3^-$  by BATs could be reduced; (ii) the production of carbonic anhydrase, used to catalyse the conversion of

$\text{CO}_2$  to  $\text{HCO}_3^-$  and  $\text{H}^+$  (Bertucci et al., 2013), could be retarded. Both these processes are significantly down-regulated during coral bleaching and thermal stress associated with the loss of symbionts (Kenkel et al., 2013; Bernardet et al., 2019). Our samples were not bleached by high temperature stress, but they did bleach due to nutrient-related stress (Fig. 1; see also Rosset et al., 2017; Buckingham et al., 2022). Nutrient imbalance is associated with a significant decline in symbiont number (Fig. 3), and with a disruption of photosynthetic efficiency, particularly for *Porites* (Fig. 4). Given that the LNLP treatment also experienced a loss of symbionts however, a decrease in the number of symbionts alone does not appear to disrupt the carbonate system in the ECM in this way. This points to the efficiency of that system (Fig. 4) being more important, as photosynthetic efficiency appears to only be disrupted in the nutrient imbalanced treatments, and not nutrient depleted conditions (as others have noted; Buckingham et al., 2022).

A link to photosynthetic efficiency finds support in studies that show seasonal trends with negatively correlated  $\text{pH}_{\text{cf}}$  and  $\text{DIC}_{\text{cf}}$ , in which greater pH upregulation has been linked to a reduced supply of photosynthetically-driven metabolic DIC associated with changes in temperature and/or light (D'Olivo and McCulloch, 2017; McCulloch et al., 2017). Furthermore, Prouty et al. (2022) recorded greater upregulation of  $\text{pH}_{\text{cf}}$  and lower  $\text{DIC}_{\text{cf}}$  for *Porites lobata* growing in high nutrient and low pH waters off the coast of Hawaii. Upregulation of pH was seen in that study as a potential coping mechanism as a response to nutrient-driven calcification stressors that oppose photosynthesis and calcification. Our simple modelling (black lines in Fig. 8) however shows that a higher  $\Delta\text{pH}$  in response to nutrient imbalance is likely due to a lower  $\text{HCO}_3^-$  flux to the ECM, possibly as photosynthetic efficiency is disrupted, which lowers the DIC of the calcifying space and correspondingly increases  $\text{pH}_{\text{cf}}$ .

#### 4.4. Potential causes of nutrient-driven changes in coral skeleton geochemistry

##### 4.4.1. Rayleigh Fractionation

The ECM is a semi-isolated space where new coral skeleton precipitates, and restriction of the inward flux of ions from ambient seawater results in a change in its chemistry as precipitation occurs: DIC and pH, as well as [Ca] and  $[\text{CO}_3]$ , decrease in the ECM until conditions

are no longer favourable for precipitation (Ram and Erez, 2021). Furthermore, elements with a partition coefficient (D) of  $>1$ , such as Ba and Sr, will decrease in the residual ECM relative to Ca as they are preferentially taken up into aragonite (Gaetani and Cohen, 2006; Ram and Erez, 2021). This results in later forming aragonite being characterised by progressively lower Ba/Ca and Sr/Ca ratios compared to that of the earlier forming aragonite. In contrast, elements with a D of  $<1$ , such as B and Mg, will increase in the residual ECM relative to Ca, with later forming aragonite being characterised by progressively higher B/Ca and Mg/Ca ratios (Gagnon et al., 2007; Stewart et al., 2016). The process, known as closed system Rayleigh-type fractionation, has sometimes been used to explain E/Ca variation within coral skeletons (Gaetani and Cohen, 2006; Cohen et al., 2009), although numerous other studies have presented data that is not consistent with this type of model (Meibom et al., 2008; Rollion-Bard et al., 2009; Brahmi et al., 2012).

The degree to which the ECM of a particular coral is isolated at a given point in time controls the degree of Rayleigh-type fraction, which in turn impacts the chemical evolution of both the ECM and the skeleton. Following that imbalanced or depleted  $[\text{NO}_3^-]$  and/or  $[\text{PO}_4^{3-}]$  impacts coral growth, it is possible that geochemical variations ( $\delta^{11}\text{B}$  and E/Ca) between the different nutrient treatments could be the result of differing degrees of Rayleigh-type fractionation. Gagnon et al. (2007) demonstrated that the E/Ca signature of *D. dianthus* aragonite in the outer septa was consistent with a Rayleigh-type fractionation model, and comparisons to such closed system models can be used to assess whether such process can explain the variation in E/Ca data (e.g. Stewart et al., 2016). Furthermore, if Rayleigh-type fractionation was a dominant process controlling the variations in E/Ca data, correlations would be expected between pairs of E/Ca ratios: positive for those with similar D values, e.g. B/Ca and Mg/Ca (both  $<1$ ), and negative for those with contrasting D values, e.g. Sr/Ca ( $>1$ ) and Mg/Ca ( $<1$ ).

Rayleigh-type fractionation models are described by the following equations (Gagnon et al., 2007):

$$\left(\frac{X}{\text{Ca}}\right)_{\text{coral}} = D_x \left(\frac{X}{\text{Ca}}\right)_{\text{sol}} F^{D_x-1} \quad (9)$$

where the extent of precipitation is defined as:

$$F = \left(\frac{[\text{Ca}]}{[\text{Ca}]_0}\right)_{\text{sol}} \quad (10)$$

Fig. 9 shows the coral E/Ca data plotted alongside theoretical closed system Rayleigh-type fractionation models for Li, B, Mg, and Sr incorporation into skeletal aragonite calculated following Eqs. (9) and (10), where  $D_{\text{Li}} = 6.60\text{E-}4$ ,  $D_{\text{B}} = 2.80\text{E-}3$ ,  $D_{\text{Mg}} = 2.35\text{E-}4$ , and  $D_{\text{Sr}} = 1.24$ , and calcifying fluid assumptions are as follows:  $[\text{Li}]_{\text{sol0}} = 26.0 \mu\text{M}$ ,  $[\text{B}]_{\text{sol0}} = 433.3 \mu\text{M}$ ,  $[\text{Mg}]_{\text{sol0}} = 52.9 \text{ mM}$ ,  $[\text{Ca}]_{\text{sol0}} = 10.3 \text{ mM}$ ,  $[\text{Sr}]_{\text{sol0}} = 91$

$\mu\text{M}$ . Whilst some of the variation within treatments may be consistent with Rayleigh-type fractionation, for example the LNHP and HNHP *A. polystoma*, variation between the treatments is not. In addition, there are no well-defined correlations between E/Ca ratios for different treatments in Fig. 9 that are consistent with their respective D values. The implication of this finding is that the nutrient treatments modify element uptake beyond a simple Rayleigh-type effect.

#### 4.4.2. Differences in [Ca]

Ram and Erez (2021) demonstrated a positive correlation between E/Ca<sub>coral</sub> and E/Ca<sub>sw</sub> for *Pocillopora damicornis* and *Acropora cervicornis* skeletons cultured under varying [Ca]<sub>sw</sub>. If imbalanced nutrients resulted in differences in [Ca] in the ECM of corals due to modification of the calcification process, then variations in [Ca] of the unobserved ECM may explain the variation in the E/Ca seen in samples from this study.

To examine this possibility, mean Li/Ca, Mg/Ca, and Sr/Ca of the four nutrient treatments have been plotted alongside E/Ca trends from Ram and Erez (2021) for both *P. damicornis* and *A. cervicornis* cultured under varying [Ca] (Fig. 10). Whilst the slopes are similar when Sr/Ca is plotted against Mg/Ca, the mean Li/Ca versus mean Mg/Ca for *P. lichen* in particular suggests that [Ca] of the unobserved ECM cannot explain the E/Ca differences between the different nutrient treatments.

#### 4.4.3. Theoretical $\text{CaCO}_3$ precipitation rates

Gabitov et al. (2011) demonstrated that the Li/Ca and Mg/Ca of spherulite fibres increases with aragonite precipitation rate. Mavromatis et al. (2015) likewise showed variations in [B] of aragonite can be accounted for by changes in precipitation rates that result from high saturation states in the calcifying fluid, whilst  $D_{\text{Sr}}$  in aragonite also changes as a function of precipitation rate, albeit this relationship is apparently also impacted by temperature (AlKhatib and Eisenhauer, 2017). Variation between the E/Ca of coral skeleton cultured in different nutrient treatments could therefore simply relate to differing skeletal precipitation rates as governed by the respective nutrient levels.

Calcification rates were not measured during culturing, however theoretical  $\text{CaCO}_3$  precipitation rates (G) can be calculated based on  $\Omega_{\text{cf}}$  (saturation state of the calcifying fluid where [Ca] is assumed to be that of the parent seawater:  $\sim 10 \text{ mM}$ ) and T following McCulloch et al. (2012a):

$$G = k(\Omega_{\text{cf}} - 1)^n \quad (11)$$

With the following temperature dependence for aragonite precipitation:

$$k_{\text{aragonite}} = -0.0177T^2 + 1.47T + 14.9 \quad (12)$$

$$n_{\text{aragonite}} = 0.0628T + 0.0985 \quad (13)$$

Calculated mean ( $\pm 2\text{SE}$ ) theoretical  $\text{CaCO}_3$  precipitation rates for

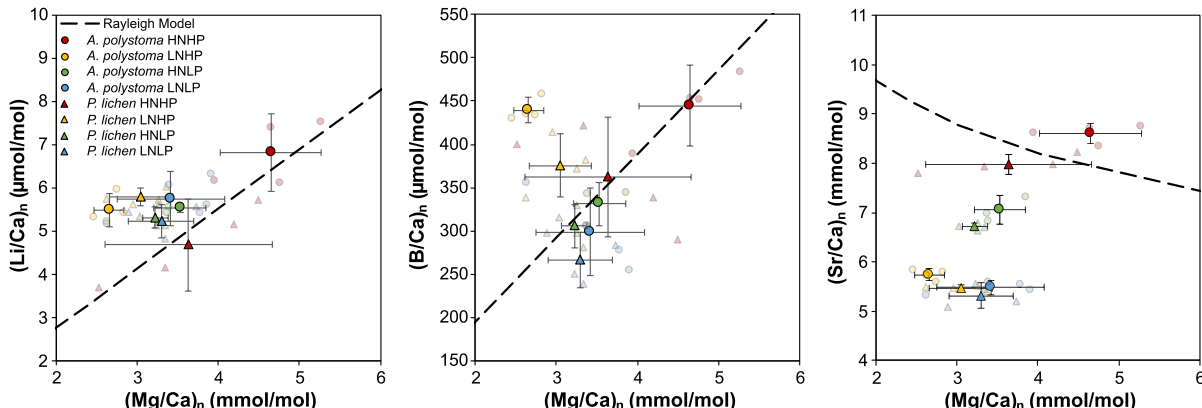
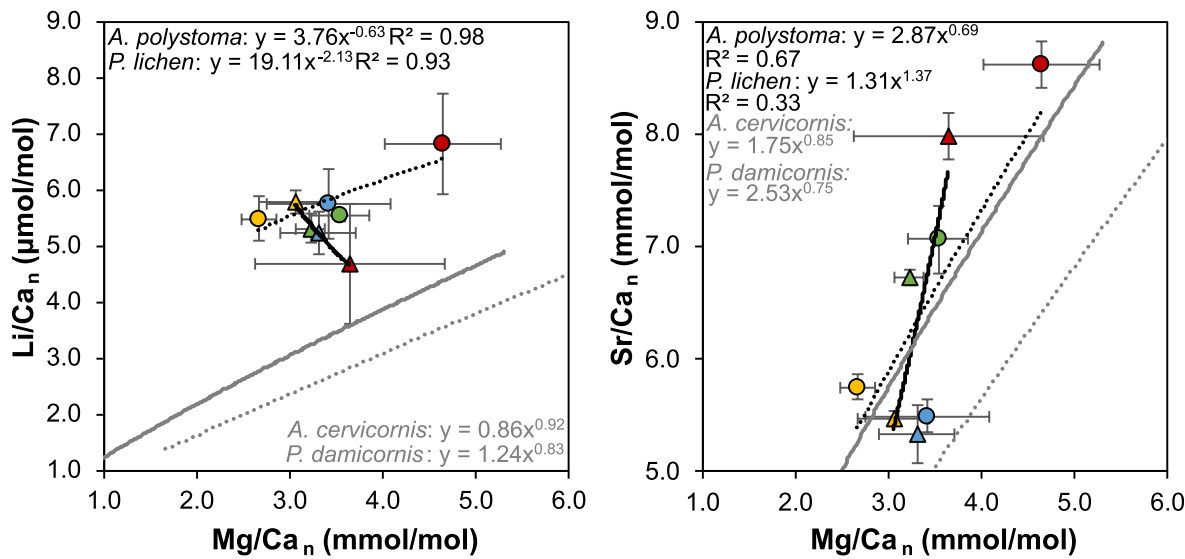


Fig. 9. Rayleigh fractionation models for Li, B, Mg and Sr incorporation into cultured *A. polystoma* and *P. lichen*.



**Fig. 10.** Mean ( $\pm 2\text{SE}$ ) Li/Ca, Mg/Ca and Sr/Ca of *A. polystoma* (circles; dashed black trendline) and *P. lichen* (triangles; solid black trendline) cultured in the four nutrient treatments alongside E/Ca trends driven by changing [Ca] for *P. damicornis* (solid grey trendline) and *A. cervicornis* (dashed grey trendline) as reported by Ram and Erez (2021). Red data points = HNHP, yellow = LNHP, green = HNLP, blue = LNLP. (For interpretation of the references to colour in this figure legend, the reader is referred to the web version of this article.)

corals grown in the replete HNHP treatment were  $4,331 \pm 818 \mu\text{mol m}^{-2} \text{hr}^{-1}$  for *A. polystoma* and  $5,514 \pm 648 \mu\text{mol m}^{-2} \text{hr}^{-1}$  for *P. lichen* (Fig. 11, Table S2). Similar rates were calculated for *A. polystoma* cultured in both imbalanced treatments, and for *P. lichen* cultured under HNLP conditions. The mean calculated rate of *P. lichen* grown under LNHP conditions was significantly lower ( $p < 0.05$ , *t*-test; Table S3) than that of *P. lichen* cultured in the HNHP treatment. Corals grown in the deplete LNLP treatment are characterised by higher mean theorised  $\text{CaCO}_3$  precipitation rates compared to those grown in the HNHP treatment, and this difference was significant ( $p < 0.05$ , *t*-test) for *A. polystoma*.

Despite marked differences in the theoretical  $\text{CaCO}_3$  precipitation rates between the nutrient treatments, relationships with the E/Ca ratios studied are poor (Fig. 11). Precipitation rate therefore cannot satisfactorily explain all the geochemical variation we observe recorded in the corals. However, it must be stressed that this is based on theoretical rates derived from  $\Omega_{\text{cf}}$  and T, rather than an actual measured quantity, and future studies should endeavour to quantify actual calcification rates to explore this issue further.

#### 4.4.4. Micro-structural biases within the coral skeleton

Scleractinian coral skeletons consist of several distinct structural

components. Primarily, these are: early mineralisation zones, also known as centres of calcification (COCs), that are the basis for initial precipitation, and bundles of acicular or fibrous crystals also referred to as fasciculi (Allison and Finch, 2007) that radiate out from these features and thicken the skeleton (Wells, 1956; Cohen et al., 2001, 2004). A number of studies have shown that Li/Ca and Mg/Ca are elevated in the COCs compared to surrounding fasciculi for a number of deep sea and tropical coral species, including *Desmophyllum dianthus*, *Lophelia pertusa*, *Porites clavus*, and *Porites lobata* (Meibom et al., 2004; Allison and Finch, 2004; Gagnon et al., 2007; Case et al., 2010; Rollion-Bard and Blamart, 2015). Sr/Ca is also typically enriched in COCs (Cohen et al., 2001; Allison and Finch, 2004; Allison et al., 2005) — although not in every case (Shirai et al., 2005; Gagnon et al., 2007). Furthermore, Li/Mg (Cuny-Guirriec et al., 2019), B/Ca and  $\delta^{11}\text{B}$  (Blamart et al., 2007; Jurikova et al., 2019) also vary structurally, but in these instances COCs are associated with lower values compared to the fasciculi.

Buckingham et al. (2022) investigated the physiological and calcification responses of *A. polystoma* to nutrient limited and enriched conditions. Alongside reduced linear extension, significant thickening of skeletal elements and reduced porosity were recorded. Although detailed micro-structural observations were not made here, it was observed that skeletal growth was much reduced under all imbalanced

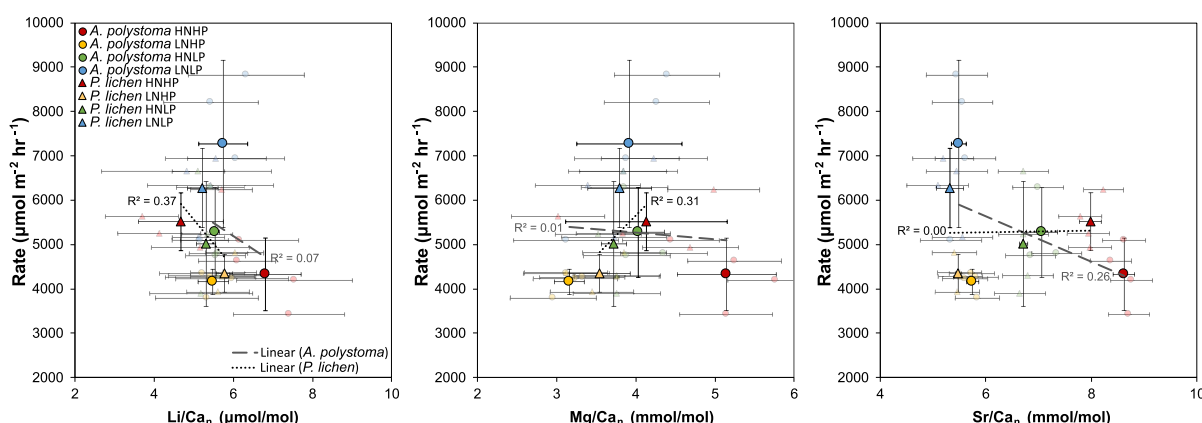


**Fig. 11.** Theoretical  $\text{CaCO}_3$  precipitation rate versus E/Ca ratios for *A. polystoma* and *P. lichen* grown in different nutrient treatments. B/Ca is not plotted because it is used to calculate  $\Omega_{\text{cf}}$ , itself used to calculate the rate (Eq. (9)).

and depleted nutrient treatments. Following that geochemical differences have frequently been reported across the complex microstructure of coral skeletons, a change in the balance of structural components between corals grown under different nutrient treatments may account for the geochemical differences reported here.

With the shift in calcification strategies towards increased thickening noted by Buckingham et al. (2022) and highlighted here, the geochemical signatures of corals grown in LNLP, HNLP and LNHP conditions would be expected to have lower Li/Ca, Mg/Ca, and possibly also Sr/Ca, alongside higher Li/Mg, B/Ca, and  $\delta^{11}\text{B}$ , compared to the replete HNHP treatment. Lower Mg/Ca and Sr/Ca, alongside higher Li/Mg, are reported here for both *A. polystoma* and *P. lichen*, whilst *A. polystoma* is also characterised by lower Li/Ca, suggesting structural biases are a possible cause of the geochemical variation observed here (Fig. 5). However, the Li/Ca of *P. lichen* counters this argument as it is higher in the nutrient deplete and imbalanced treatments compared to the replete. Yet species-specific differences cannot be ruled out at this stage and a better understanding of *P. lichen* thickening rates is required for a full understanding. What is apparent is that like *A. polystoma*, the growth strategies of *P. lichen* also changed due to nutrient depletion and enrichment (Fig. 2), therefore a degree of change in the rate of thickening is entirely plausible for this species too. Differences in the B/Ca and  $\delta^{11}\text{B}$  of corals cultured in the nutrient treatments are also not easily explained this way, suggesting that the carbonate system is perhaps responding in additional ways overriding any structural effect (see Section 4.3). Indeed, the coherent trends we observe between  $\Delta[\text{DIC}]$  and  $\Delta\text{pH}$  suggest the nutrient treatments impact the carbonate system over and above any changes in  $\delta^{11}\text{B}$  and B/Ca relating to a changing balance in structural components (Fig. 8).

Nutrient depletion or imbalanced enrichment clearly alters the calcification strategy of corals (e.g. Buckingham et al., 2022; this study) in such a way as to result in increased skeletal thickening, an observation that is consistent with ideas linking nutrient depletion with higher calcification rates (McConaughey, 2012). Given the enrichment of organic molecules (and proteins in particular) in COCs (e.g. Gautret et al., 2000; Cuif et al., 2003; DeCarlo et al., 2018), and the potential role of organic proteins (e.g. coral acid-rich proteins or CARPs, Mass et al., 2013) in nucleation and hence formation of COCs, it is possible that nutrient depletion and nutrient imbalance disrupts this aspect of coral growth in particular. The organic content of fasciculi associated with skeletal thickening is typically lower (e.g. DeCarlo et al., 2018), and as such it is possible that the growth of this structural component is not as affected by nutrient imbalance or depletion. While this is an intriguing possibility for explaining the geochemical differences presented here for *A. polystoma* and *P. lichen* cultured in different nutrient treatments, this hypothesis requires further testing. Future studies that combine detailed skeletal growth measurements, including skeletal thickening, and high-resolution geochemical analysis that can target both COCs and fasciculi separately, are specifically required.

## 5. Conclusion

Imbalanced enrichment and depletion of nitrate and phosphate can change coral skeletal chemistry, impacting geochemical inferences about ocean temperature and pH: temperature proxies Sr/Ca, Mg/Ca, and Li/Mg recorded in corals cultured under extreme imbalanced and deplete nutrient conditions gave reconstructed temperatures biased by  $-7^\circ\text{C}$  to  $+52^\circ\text{C}$  compared to corals cultured in the replete treatment, whilst induced changes in  $\delta^{11}\text{B}$  exceeded the equivalent of the 0.1 pH unit change so far caused by anthropogenic acidification of the ocean. Particular care is therefore needed when samples derive from regions where nutrient budgets have been disturbed by anthropogenic activity, although nutrient proxies such as P/Ca, or multiple E/Ca proxies which have divergent responses to nutrient stress, could be employed to identify or mitigate against these influences.

Nutrient depletion or imbalanced enrichment also alters the

calcification strategy of corals, leading to a reduction in extension and an increase in thickening and encrusting growth. In addition, corals cultured in nutrient imbalanced conditions recorded a decline in their photosynthetic efficiency, with a decrease in photosynthetically-driven DIC flux to the ECM considered a likely driver of disruption to the carbonate system for corals cultured under such conditions. While the relationship between nutrients, changing skeletal growth morphology, and the ECM carbonate system requires further study, taken together our observations suggest different environmental sensitivities exist for different aspects of the coral biomineralisation toolkit, and ultimately it is this that underpins the response of the phenotype to environmental change.

## Declaration of Competing Interest

The authors declare that they have no known competing financial interests or personal relationships that could have appeared to influence the work reported in this paper.

## Acknowledgements

We thank Robbie Robinson and George Clarke for their support in the maintenance of the experimental aquarium systems of the Coral Reef Laboratory, Dan Doran and Matthew Beverley-Smith are gratefully acknowledged for sample preparation, whilst Andy Milton and Mathew Cooper are thanked for their analytical support. This work was funded by the Leverhulme Trust that supported CDS and TBC, and ERC Advanced Grant Micons2Reefs (#884650), both awarded to GLF. We also acknowledge funding from NERC (Defining Nutritional Bottlenecks of Reef Coral Growth and Stress Tolerance—NE/T001364/1) to JW and CDA.

## Appendix A. Supplementary material

This file contains data tables relating to the composition of culture waters (Table S1), the geochemical composition of cultured coral samples (Table S2), the results of t-tests (Table S3), the skeletal growth of *A. polystoma* and *P. lichen* during culturing (Table S4), the density of zooxanthellae on *A. polystoma* and *P. lichen* during culturing (Table S5), the photosynthetic efficiency of coral zooxanthellae during culturing (Table S6); and cross plots of E/Ca and  $\delta^{11}\text{B}$  data for the cultured *A. polystoma* (Fig. S1) and *P. lichen* (Fig. S2). Supplementary material to this article can be found online at <https://doi.org/10.1016/j.gca.2023.04.011>.

## References

- AlKhatib, M., Eisenhauer, A., 2017. Calcium and strontium isotope fractionation during precipitation from aqueous solutions as a function of temperature and reaction rate; II. Aragonite. *Geochim. Cosmochim. Acta* 209, 320–342.
- Allison, N., Finch, A.A., 2004. High-resolution Sr/Ca records in modern *Porites lobata* corals: Effects of skeletal extension rate and architecture. *Geochem. Geophys. Geosyst.* 5, Q05001.
- Allison, N., Finch, A.A., Newville, M., Sutton, S.R., 2005. Strontium in coral aragonite: 3. Sr co-ordination in relation to skeletal architecture. *Geochim. Cosmochim. Acta* 69, 3801–3811.
- Allison, N., Finch, A.A., 2007. High temporal resolution Mg/Ca and Ba/Ca records in modern *Porites lobata* corals. *Geochem. Geophys. Geosyst.* 8, Q05001.
- Alpert, A.E., Cohen, A.L., Oppo, D.W., DeCarlo, T.M., Gove, J.M., Young, C.W., 2016. Comparison of equatorial Pacific sea surface temperature variability and trends with Sr/Ca records from multiple corals. *Paleoceanogr. Paleoclimatol.* 31, 252–265.
- Aston, E.A., Williams, G.J., Green, J.M., Davies, A.J., Wedding, L.M., Gove, J.M., Jouffray, J.B., Jones, T.T., Clark, J., 2019. Scale-dependent spatial patterns in benthic communities around a tropical island seascapes. *Ecography* 42, 578–590.
- Atkinson, M.J., Carlson, B., Crow, G.L., 1995. Coral growth in high-nutrient, low-pH seawater: a case study of corals cultured at the Waikiki Aquarium, Honolulu, Hawaii. *Coral Reefs* 14, 215–223.
- Beck, J.W., Edwards, R.L., Ito, E., Taylor, F.W., Recy, J., Rougerie, F., Joannot, P., Henin, C., 1992. Sea-surface temperature from coral skeletal strontium/calcium ratios. *Science* 257, 644–647.
- Becker, D.M., Silbiger, N.J., 2020. Nutrient and sediment loading affect multiple facets of coral functionality in a tropical branching coral. *J. Exp. Biol.* 223, jeb.225045.

Bell, P., Tomascik, T., 1993. The demise of the coral fringing reefs of Barbados and of regions in the Great Barrier Reef (GBR) lagoon – impacts of eutrophication. Proceedings of the colloquium on global aspects of coral reefs: health, hazards and history, Ginsburg RN compiler, Rosenstiel School of Marine and Atmospheric Science, University of Miami, pp. 319–325.

Bell, P.R.F., Elmets, I., Uwins, P., 1999. Nitrogen fixation by *Trichodesmium* spp. in the Central and Northern Great Barrier Reef Lagoon: relative importance of the fixed-nitrogen load. *Mar. Ecol. Prog. Ser.* 186, 119–126.

Bernardet, C., Tambutté, E., Techer, N., Tambutté, S., Venn, A.A., 2019. Ion transporter gene expression is linked to the thermal sensitivity of calcification in the reef coral *Stylophora pistillata*. *Sci. Rep.* 9, 18676.

Bertucci, A., Moya, A., Tambutté, S., Allemand, D., Supuran, C.T., Zoccola, D., 2013. Carbonic anhydrases in anthozoan corals—A review. *Bioorg. Med. Chem.* 21, 1437–1450.

Blamart, D., Rollion-Bard, C., Meibom, A., Cuif, J.-P., Juillet-Leclerc, A., Dauphin, Y., 2007. Correlation of boron isotopic composition with ultrastructure in the deep-sea coral *Lophelia pertusa*: Implications for biomineralization and paleo-pH. *Geochem. Geophys. Geosyst.* 8, Q12001.

Bongiorni, L., Shafir, S., Angel, D., Rinkevich, B., 2003. Survival, growth and gonad development of two hermatypic corals subjected to in situ fish-farm nutrient enrichment. *Mar. Ecol. Prog. Ser.* 253, 137–144.

Brahmi, C., Kopp, C., Domart-Coulon, I., Stolarski, J., Meibom, A., 2012. Skeletal growth dynamics linked to trace-element composition in the scleractinian coral *Pocillopora damicornis*. *Geochim. Cosmochim. Acta* 99, 146–158.

Branson, O., 2018. Boron Incorporation into Marine CaCO<sub>3</sub>. In: Marschall, H.R., Foster, G.L. (Eds.), *Boron Isotopes*. Springer, Cham, pp. 71–105.

Brodie, J.E., Kroon, F.J., Schafelke, B., Wolanski, E.C., Lewis, S.E., Devlin, M.J., Bohnet, I.C., Bainbridge, Z.T., Waterhouse, J., Davis, A.M., 2012. Terrestrial pollutant runoff to the Great Barrier Reef: An update of issues, priorities and management responses. *Mar. Pollut. Bull.* 65, 81–100.

Buckingham, M.C., D'Angelo, C., Chalk, T.B., Foster, G.L., Johnson, K.G., Connelly, Z., Olla, C., Saeed, M., Wiedenmann, J., 2022. Impact of nitrogen (N) and phosphorus (P) enrichment and skewed N: P stoichiometry on the skeletal formation and microstructure of symbiotic reef corals. *Coral Reefs* 41, 1147–1159.

Case, D.H., Robinson, L.F., Auro, M.E., Gagnon, A.C., 2010. Environmental and biological controls on Mg and Li in deep-sea scleractinian corals. *Earth Planet. Sci. Lett.* 300, 215–225.

Catanzaro, E.J., Champion, C.E., Garner, E.L., Marinenko, G., Sappenfield, K.M., Shields, W.R., 1970. *Boric assay; isotopic, and assay standard reference materials*. Washington, DC: National Bureau of Standards. Special Publication 260–17.

Chalk, T.B., Standish, C.D., D'Angelo, C., Castillo, K.D., Milton, J.A., Foster, G.L., 2021. Mapping coral calcification strategies from in situ boron isotope and trace element measurements of the tropical coral *Siderastrea siderea*. *Sci. Rep.* 11, 472.

Cohen, A.L., Layne, G.D., Hart, S.R., Lobel, P.S., 2001. Kinetic control of skeletal Sr/Ca in a symbiotic coral: Implications for the paleotemperature proxy. *Paleoceanogr. Paleoclimatol.* 16, 20–26.

Cohen, A.L., Smith, S.R., McCartney, M.S., van Etten, J., 2004. How brain corals record climate: an integration of skeletal structure, growth and chemistry of *Diploria labyrinthiformis* from Bermuda. *Mar. Ecol. Prog. Ser.* 271, 147–158.

Cohen, A.L., McCorkle, D.C., de Putron, S., Gaetani, G.A., Rose, K.A., 2009. Morphological and compositional changes in the skeletons of new coral recruits reared in acidified seawater: Insights into the biomineralization response to ocean acidification. *Geochim. Geophys. Geosyst.* 10, Q07005.

Corrège, T., 2006. Sea surface temperature and salinity reconstruction from coral geochemical tracers. *Palaeogeogr. Palaeoclimatol. Palaeoecol.* 232, 408–428.

Costa, C.F., Sassi, R., Amaral, F.D., 2005. Annual cycle of symbiotic dinoflagellates from three species of scleractinian corals from coastal reefs of northeastern Brazil. *Coral Reefs* 24, 191–193.

Crossland, C., Barnes, D., 1977. Nitrate assimilation enzymes from two hard corals, *Acropora acuminata* and *Goniastrea australensis*. *Comp. Biochem. Physiol. B: Comp. Biochem.* 57, 151–157.

Cuif, J.-P., Dauphin, Y., Doucet, J., Salome, M., Susini, J., 2003. XANES mapping of organic sulfate in three scleractinian coral skeletons. *Geochim. Cosmochim. Acta* 67, 75–83.

Cuny-Guirriec, K., Douville, E., Reynaud, S., Allemand, D., Bordier, L., Canesi, M., Mazzoli, C., Taviani, M., Canese, S., McCulloch, M., Trotter, J., Rico-Esparo, S.D., Sanchez-Cabeza, J.-A., Ruiz-Fernández, A.C., Carricart-Ganivet, J.P., Scott, P.M., Sadekov, A., Montagna, P., 2019. Coral Li/Mg thermometry: Caveats and constraints. *Chem. Geol.* 523, 162–178.

D'Angelo, C., Wiedenmann, J., 2012. An experimental mesocosm for long-term studies of reef corals. *J. Mar. Biol. Assoc. U. K.* 92, 769–775.

D'Angelo, C., Wiedenmann, J., 2014. Impacts of nutrient enrichment on coral reefs: new perspectives and implications for coastal management and reef survival. *Curr. Opin. Environ. Sust.* 7, 82–93.

D'Olivo, J.P., Ellwood, G., DeCarlo, T.M., McCulloch, M.T., 2019. Deconvolving the long-term impacts of ocean acidification and warming on coral biomineralization. *Earth Planet. Sci. Lett.* 526, 115785.

D'Olivo, J.P., McCulloch, M.T., 2017. Response of coral calcification and calcifying fluid composition to thermally induced bleaching stress. *Sci. Rep.* 7, 1–15.

DeCarlo, T.M., Ren, H., Farfan, G.A., 2018. The origin and role of organic matrix in coral calcification: insights from comparing coral skeleton and abiogenic aragonite. *Front. Mar. Sci.* 5, 170.

DeCarlo, T.M., Gajdzik, L., Ellis, J., Coker, D.J., Roberts, M.B., Hammerman, N.M., Pandolfi, J.M., Monroe, A.A., Berumen, M.L., 2020. Nutrient-supplying ocean currents modulate coral bleaching susceptibility. *Sci. Adv.* 6, eabc5493.

DeGeorges, A., Goreau, T.J., Reilly, B., 2010. Land-sourced pollution with an emphasis on domestic sewage: Lessons from the Caribbean and implications for coastal development on Indian Ocean and Pacific coral reefs. *Sustainability* 2, 2919–2949.

Devlin, M.J., Brodie, J., 2005. Terrestrial discharge into the Great Barrier Reef Lagoon: nutrient behavior in coastal waters. *Mar. Pollut. Bull.* 51, 9–22.

Dickson, A.G., 1990. Thermodynamics of the dissociation of boric acid in synthetic seawater from 273.15 to 318.15 K. *Deep Sea Res. Part I* 37, 755–766.

Dickson, A.G., Sabine, C.L., Christian, J.R., 2007. Guide to best practices for ocean CO<sub>2</sub> measurements, PICES Special Publication 3, IOC report No. 8, 191 pp.

Dollar, S., 1994. Sewage discharge on coral reefs: not always pollution. *Coral Reefs* 13, 224.

Dubinsky, Z., Jokiel, P.L., 1994. Ratio of Energy and Nutrient Fluxes Regulates Symbiosis between Zooxanthellae and Corals. *Pac. Sci.* 48, 313–324.

Dubinsky, Z., Stambler, N., Ben Zion, M., McCloskey, L.R., Muscatine, L., Falkowski, P.G., 1990. The effect of external nutrient resources on the optical properties and photosynthetic efficiency of *Stylophora pistillata*. *Proc. R. Soc. B* 239, 231–246.

Dunn, J.G., Sammarco, P.W., LaFleur Jr., G., 2012. Effects of phosphate on growth and skeletal density in the scleractinian coral *Acropora muricata*: a controlled experimental approach. *J. Exp. Mar. Biol. Ecol.* 411, 34–44.

Fabricius, K.E., 2005. Effects of terrestrial runoff on the ecology of corals and coral reefs: review and synthesis. *Mar. Pollut. Bull.* 50, 125–146.

Fagoonee, I., Wilson, H.B., Hassell, M.P., Turner, J.R., 1999. The Dynamics of Zooxanthellae Populations: A Long-Term Study in the Field. *Science* 283, 843–845.

Fallon, S.J., McCulloch, M.T., Albert, C., 2003. Examining water temperature proxies in Porites corals from the Great Barrier Reef: a cross-shelf comparison. *Coral Reefs* 22, 389–404.

Frerri-Pagès, C., Gattuso, J.P., Dallot, S., Jaubert, J., 2000. Effect of nutrient enrichment on growth and photosynthesis of the zooxanthellate coral *Stylophora pistillata*. *Coral Reefs* 19, 103–113.

Finch, A.A., Allison, N., 2008. Mg structural state in coral aragonite and implications for the paleoenvironmental proxy. *Geophys. Res. Lett.* 35, L08704.

Foster, G.L., 2008. Seawater pH, pCO<sub>2</sub> and CO<sub>3</sub> 2- variations in the Caribbean Sea over the last 130 kyr: A boron isotope and B/Ca study of planktic foraminifera. *Earth Planet. Sci. Lett.* 271, 254–266.

Foster, G.L., Pogge von Strandmann, P.A.E., Rae, J.W.B., 2010. Boron and magnesium isotopic composition of seawater. *Geochim. Geophys. Geosyst.* 11, Q08015.

Foster, G.L., Hönisch, B., Paris, G., Dwyer, G.S., Rae, J.W.B., Elliott, T., Gaillardet, J., Hemming, N.G., Louvat, P., Vengosh, A., 2013. Interlaboratory comparison of boron isotope analyses of boric acid, seawater and marine CaCO<sub>3</sub> by MC-ICPMS and NTIMS. *Chem. Geol.* 358, 1–14.

Fowell, S.E., Foster, G.L., Ries, J.B., Castillo, K.D., de la Vega, E., Tyrrell, T., Donald, H.K., Chalk, T.B., 2018. Historical trends in pH and carbonate biogeochemistry on the Belize Mesoamerican barrier reef system. *Geophys. Res. Lett.* 45, 3228–3237.

Furnas, M., Mitchell, A., Skuza, M., Brodie, J., 2005. In the other 90%: Phytoplankton responses to enhanced nutrient availability in the Great Barrier Reef Lagoon. *Mar. Pollut. Bull.* 51, 253–265.

Gabitov, R.I., Schmitt, A.K., Rosner, M., McKeegan, K.D., Gaetani, G.A., Cohen, A.L., Watson, E.B., Harrison, T.M., 2011. In situ <sup>8</sup>Li, Li/Ca, and Mg/Ca analyses of synthetic aragonites. *Geochem. Geophys. Geosyst.* 12, Q03001.

Gaetani, G.A., Cohen, A.L., 2006. Element partitioning during precipitation of aragonite from seawater: A framework for understanding paleoproxies. *Geochim. Cosmochim. Acta* 70, 4617–4634.

Gaetani, G.A., Cohen, A.L., Wang, Z., Crusius, J., 2011. Rayleigh-based, multi-element coral thermometry: A biomineralization approach to developing climate proxies. *Geochim. Cosmochim. Acta* 75, 1920–1932.

Gagnon, A.C., Adkins, J.F., Fernandez, D.P., Robinson, L.F., 2007. Sr/Ca and Mg/Ca vital effects correlated with skeletal architecture in a scleractinian deep-sea coral and the role of Rayleigh fractionation. *Earth Planet. Sci. Lett.* 261, 280–295.

Gagnon, A.C., Adkins, J.F., Erez, J., 2012. Seawater transport during coral biomineralization. *Earth Planet. Sci. Lett.* 329–330, 150–161.

Gattuso, J.-P., Epitalon, J.-M., Lavigne, H., Orr, J., Gentili, B., Hagens, M., Hofmann, A., Mueller, J.-D., Proye, A., Rae, J., Soetaert, K., 2021. Package 'seacarb': seawater carbonate chemistry. R Package Version 3 (3).

Gautret, P., Cuif, J.-P., Stolarski, J., 2000. Organic components of the skeleton of scleractinian corals: evidence from in situ acridine orange staining. *Acta Palaeontol. Pol.* 45, 107–118.

Gilbert, P., Bergmann, K.D., Boekelheide, N., Tambutte, S., Mass, T., Marin, F., Adkins, J.F., Erez, J., Gilbert, B., Knutson, V., Cantine, M., Hernandez, J.O., Knoll, A.H., 2022. Biomineralization: integrating mechanism and evolutionary history. *Sci. Adv.* 8, eabl9653.

Godinot, C., Ferri-Pagès, C., Grover, R., 2009. Control of phosphate uptake by zooxanthellae and host cells in the scleractinian coral *Stylophora pistillata*. *Limnol. Oceanogr.* 54, 1627–1633.

Godinot, C., Houlbréque, F., Grover, R., Ferri-Pagès, C., 2011. Coral Uptake of Inorganic Phosphorus and Nitrogen Negatively Affected by Simultaneous Changes in Temperature and pH. *PLoS ONE* 6, e25024.

Gorbunov, M.Y., Kolber, Z.S., Lesser, M.P., Falkowski, P.G., 2001. Photosynthesis and photoprotection in symbiotic corals. *Limnol. Oceanogr.* 46, 75–85.

Grover, R., Maguer, J., Allemand, D., Ferri-Pagès, C., 2003. Nitrate uptake in the scleractinian coral *Stylophora pistillata*. *Limnol. Oceanogr.* 48, 2266–2274.

Guo, W., 2019. Seawater temperature and buffering capacity modulate coral calcifying pH. *Sci. Rep.* 9, 1189.

Gutjahr, M., Bordier, L., Douville, E., Farmer, J., Foster, G.L., Hathorne, E.C., Hönisch, B., Lemarchand, D., Louvat, P., McCulloch, M., Noireaux, J., Pallavicini, N., Rae, J.W.B., Rodushkin, I., Roux, P., Stewart, J.A., Thil, F., You, C.-F., 2020. Sub-Permil

Interlaboratory Consistency for Solution-Based Boron Isotope Analyses on Marine Carbonates. *Geostand. Geoanal. Res.* 45, 59–75.

Hathorne, E.C., Gagnon, A., Felis, T., Adkiins, J., Asami, R., Boer, W., Caillon, N., Case, D., Cobb, K.M., Douville, E., de Menocal, P., Eisenhauer, A., Garbe-Schönberg, D., Geibert, W., Hemming, N.G., Hanson, G.N., 2013. Boron isotopic composition and concentration in modern marine carbonates. *Geochim. Cosmochim. Acta* 56, 537–543.

Henehan, M.J., Foster, G.L., Rae, J.W.B., Prentice, K.C., Erez, J., Bostock, H.C., Marshall, B.J., Wilson, P.A., 2015. Evaluating the utility of B/Ca ratios in planktic foraminifera as a proxy for the carbonate system: A case study of *Globigerinoides ruber*. *Geochem. Geophys. Geosyst.* 16, 1052–1069.

Hoegh-Guldberg, O., Smith, G.J., 1989. Influence of the population density of zooxanthellae and supply of ammonium on the biomass and metabolic characteristics of the reef corals *Seriatopora hystrix* and *Stylophora pistillata*. *Mar. Ecol. Prog. Ser.* 57 (2), 173–186.

Holcomb, M., DeCarlo, T., Gaetani, G., McCulloch, M., 2016. Factors affecting B/Ca ratios in synthetic aragonite. *Chem. Geol.* 437, 67–76.

Houlbréque, F., Ferrier-Pagès, C., 2009. Heterotrophy in tropical scleractinian corals. *Biol. Rev.* 84, 1–17.

Houlbréque, F., Tambutte, E., Ferrier-Pagès, C., 2003. Effects of zooplankton availability on the rates of photosynthesis, and tissue and skeletal growth in the Scleractinian coral *Stylophora pistillata*. *J. Exp. Mar. Biol. Ecol.* 296, 145–166.

Inoue, M., Nohara, M., Okai, T., Suzuki, A., Kawahata, H., 2004. Concentrations of Trace Elements in Carbonate Reference Materials Coral JCp-1 and Giant Clam JCt-1 by Inductively Coupled Plasma-Mass Spectrometry. *Geostand. Geoanal. Res.* 28, 411–416.

Ip, Y.K., Lim, A.L.L., Lim, R.W.L., 1991. Some properties of calcium-activated adenosine triphosphatase from the hermatypic coral *Galaxea fascicularis*. *Mar. Biol.* 111, 191–197.

Jochum, K.P., Weis, U., Stoll, B., Kuzmin, D., Yang, Q., Raczek, I., Jacob, D.E., Stracke, A., Birbaum, K., Frick, D.A., Günther, D., Enzweiler, J., 2011. Determination of Reference Values for NIST SRM 610–617 Glasses Following ISO Guidelines. *Geostand. Geoanal. Res.* 35, 397–429.

Jurikova, H., Liebetrau, V., Raddatz, J., Fietzke, J., Trotter, J., Rocholl, A., Krause, S., McCulloch, M., Rüggeberg, A., Eisenhauer, A., 2019. Boron isotope composition of the cold-water coral *Lophelia pertusa* along the Norwegian margin: Zooming into a potential pH-proxy by combining bulk and high-resolution approaches. *Chem. Geol.* 513, 143–152.

Kenkel, C.D., Meyer, E., Matz, M.V., 2013. Gene expression under chronic heat stress in populations of the mustard hill coral (*Porites astreoides*) from different thermal environments. *Mol. Ecol.* 22, 4322–4334.

Kleypas, J.A., McManus, J.W., Menez, L.A.B., 1999. Environmental limits to coral reef development: where do we draw the line? *Am. Zool.* 39, 146–159.

Klochko, K., Kaufman, A.J., Yao, W.S., Byrne, R.H., Tossell, J.A., 2006. Experimental measurement of boron isotope fractionation in seawater. *Earth Planet. Sci. Lett.* 248, 276–285.

Koop, K., Booth, D., Broadbent, A., Brodie, J., Bucher, D., Capone, D., Coll, J., Dennison, W., Erdmann, M., Harrison, P., Hoegh-Guldberg, O., Hutchings, P., Jones, G.B., Larkum, A.W.D., O’Neil, J., Steven, A., Tenter, E., Ward, S., Williamson, J., Yellowlees, D., 2001. ENCORE: the effect of nutrient enrichment on coral reefs. Synthesis of results and conclusions. *Mar. Pollut. Bull.* 42, 91–120.

Krief, S., Hendy, E.J., Fine, M., Yam, R., Meibom, A., Foster, G.L., Shemesh, A., 2010. Physiological and isotopic responses of scleractinian corals to ocean acidification. *Geochim. Cosmochim. Acta* 74, 4988–5001.

Lapointe, B.E., Brewton, R.A., Herren, L.W., Porter, J.W., Hu, C., 2019. Nitrogen enrichment, altered stoichiometry, and coral reef decline at Looe Key, Florida Keys, USA: a 3-decade study. *Mar. Biol.* 166, 108.

LaVigne, M., Matthews, K.A., Grottoli, A.G., Cobb, K.M., Anagnostou, E., Cabioch, G., Sherrell, R.M., 2010. Coral skeleton P/Ca proxy for seawater phosphate: Multi-colony calibration with a contemporaneous seawater phosphate record. *Geochim. Cosmochim. Acta* 74, 1282–1293.

Le Roux, P.J., Shirley, S.B., Benton, L., Hauri, E.H., Mock, T.D., 2004. In situ, multiple multiplier, laser ablation ICP-MS measurement of boron isotopic composition ( $\delta^{11}\text{B}$ ) at the nanogram level. *Chem. Geol.* 203, 123–138.

Lea, D.W., Shen, G.T., Boyle, E.A., 1989. Coralline barium records temporal variability in equatorial pacific upwelling. *Nature* 340, 373–376.

Lee, K., Kim, T.-W., Byrne, R.H., Millero, F.J., Feely, R.A., Liu, Y.-M., 2010. The universal ratio of boron to chlorinity for the North Pacific and North Atlantic oceans. *Geochim. Cosmochim. Acta* 74, 1801–1811.

Li, Y.-H., 1991. Distribution patterns of the elements in the ocean: A synthesis. *Geochim. Cosmochim. Acta* 55, 3223–3240.

Loya, Y., 2004. The coral reefs of Eilat—past, present and future: three decades of coral community structure studies. In: Rosenberg, E., Loya, Y. (Eds.), *Coral Reef Health and Disease*. Springer, Berlin, pp. 1–34.

Maina, J., de Moel, H., Zinke, J., Madin, J., McClanahan, T., Vermaat, J.E., 2012. Human deforestation outweighs future climate change impacts of sedimentation on coral reefs. *Nat. Commun.* 4, 1986.

Marubini, F., Davies, P.S., 1996. Nitrate increases zooxanthellae population density and reduces skeletogenesis in corals. *Mar. Biol.* 127, 319–328.

Mass, T., Drake, J.L., Haramaty, L., Kim, J.D., Zelzion, E., Bhattacharya, D., Falkowski, P.G., 2013. Cloning and characterization of four novel coral acid-rich proteins that precipitate carbonates in vitro. *Curr. Biol.* 23, 1126–1131.

Mass, T., Giuffre, A.J., Sun, C.-Y., Stifler, C.A., Frazier, M.J., Neder, M., Tamura, N., Stan, C.V., Marcus, M.A., Gilbert, P.U.P.A., 2017. Amorphous calcium carbonate particles form coral skeletons. *PNAS* 114, E7670–E7678.

Mavromatis, V., Montouillout, V., Noireaux, J., Gaillardet, J., Schott, J., 2015. Characterization of boron incorporation and speciation in calcite and aragonite from co-precipitation experiments under controlled pH, temperature and precipitation rate. *Geochim. Cosmochim. Acta* 150, 299–313.

McConaughey, T.A., 2012. Zooxanthellae that open calcium channels: implications for reef corals. *Mar. Ecol. Prog. Ser.* 460, 277–287.

McCulloch, M.T., D’Olivo, J.P., Falter, J., Holcomb, M., Trotter, J.A., 2017. Coral calcification in a changing world and the interactive dynamics of pH and DIC upregulation. *Nat. Commun.* 8, 1–8.

McCulloch, M., Fallon, S., Wyndam, T., Hendy, E., Lough, J., Barnes, D., 2003. Coral record of increased sediment flux to the inner Great Barrier Reef since European settlement. *Nature* 421, 727–730.

McCulloch, M., Trotter, J., Montagna, P., Falter, J., Dunbar, R., Freiwald, A., Försterra, G., López Correa, M., Maier, C., Rüggeberg, A., Taviani, M., 2012a. Resilience of cold-water scleractinian corals to ocean acidification: Boron isotopic systematics of pH and saturation state up-regulation. *Geochim. Cosmochim. Acta* 87, 21–34.

McCulloch, M., Falter, J., Trotter, J., Montagna, P., 2012b. Coral resilience to ocean acidification and global warming through pH up-regulation. *Nat. Clim. Change* 2, 623–627.

Meibom, A., Cuif, J.-P., Hillion, F., Constantz, B.R., Juillet-Leclerc, A., Dauphin, Y., Watanabe, T., Dunbar, R.B., 2004. Distribution of magnesium in coral skeleton. *Geophys. Res. Lett.* 31, L23306.

Meibom, A., Cuif, J.-P., Mostefaoui, S., Dauphin, Y., Houlbreque, F., Meibom, K., Dunbar, R., 2008. Compositional variations at ultra-structure length scales in coral skeleton. *Geochim. Cosmochim. Acta* 72, 1555–1569.

Millero, F.J., Feistel, R., Wright, D.G., McDougall, T.J., 2008. The composition of Standard Seawater and the definition of the Reference-Composition Salinity Scale. *Deep Sea Res. Part I* 55 (1), 50–72.

Mitchell, A.W., Reghennani, J.R., Furnas, M.J., 2001. Nitrogen levels in the Tully River — a long-term view. *Water Sci. Technol.* 43, 99–105.

Mitsuguchi, T., Matsumoto, E., Abe, O., Uchida, T., Isdale, P.J., 1996. Mg/Ca thermometry in coral skeletons. *Science* 274, 961–963.

Montagna, P., McCulloch, M., Douville, E., López Correa, M., Trotter, J., Rodolfo-Metalpa, R., Dillard, D., Ferrier-Pagès, C., Frank, N., Freiwald, A., Goldstein, S., Mazzoli, C., Reynaud, S., Rüggeberg, A., Russo, S., Taviani, M., 2014. Li/Mg systematics in scleractinian corals: Calibration of the thermometer. *Geochim. Cosmochim. Acta* 132, 288–310.

Muscatine, L., D’Elia, C.F., 1978. The uptake, retention and release of ammonium by reef corals. *Limnol. Oceanogr.* 23, 725–734.

Prouty, N.G., Wall, M., Fietzke, J., Cheriton, O.M., Agnastou, E., Phillips, B.L., Paytan, A., 2022. The role of pH up-regulation in response to nutrient-enriched, low-pH groundwater discharge. *Mar. Chem.* 243, 104134.

Ram, S., Erez, J., 2021. The distribution coefficients of major and minor elements in coral skeletons under variable calcium seawater concentrations. *Front. Earth Sci.* 9, 657176.

Rollion-Bard, C., Blamart, D., 2015. Possible controls on Li, Na, and Mg incorporation into aragonite coral skeletons. *Chem. Geol.* 396, 98–111.

Rollion-Bard, C., Vigier, N., Meibom, A., Blamart, D., Reynaud, S., Rodolfo-Metalpa, R., Martin, S., Gattuso, J.P., 2009. Effect of environmental conditions and skeletal ultrastructure on the Li isotopic composition of scleractinian corals. *Earth Planet. Sci. Lett.* 286, 63–70.

Ross, C.L., DeCarlo, T.M., McCulloch, M.T., 2019. Calibration of Sr/Ca, Li/Mg and Sr-U paleothermometry in branching and foliose corals. *Paleoceanogr. Paleoclimatol.* 34, 1271–1291.

Rosset, S., D’Angelo, C., Wiedenmann, J., 2015. Ultrastructural biomarkers in symbiotic algae reflect the availability of dissolved inorganic nutrients and particulate food to the reef coral holobiont. *Front. Earth Sci.* 2, 1–10.

Rosset, S., Wiedenmann, J., Reed, A.J., D’Angelo, C., 2017. Phosphate deficiency promotes coral bleaching and is reflected by the ultrastructure of symbiotic dinoflagellates. *Mar. Pollut. Bull.* 118, 180–187.

Sebens, K.P., Vandersall, K.S., Savina, L.A., Graham, K.R., 1996. Zooplankton capture by two scleractinian corals *Madracis mirabilis* and *Montastrea cavernosa* in a field enclosure. *Mar. Biol.* 127, 303–317.

Sevilgen, D.S., Venn, A.A., Hu, M.Y., Tambutte, E.T., de Beer, D., Planas-Bielsa, V., Tambutte, S., 2019. Full in vivo characterization of carbonate chemistry at the site of calcification in corals. *Sci. Adv.* 5, eaau7447.

Shirai, K., Kusakabe, M., Nakai, S., Ishii, T., Watanabe, T., Hiyagon, H., Sano, Y., 2005. Deep-sea coral geochemistry: Implication for the vital effect. *Chem. Geol.* 224, 212–222.

Sinclair, D.J., 2005. Correlated trace element “vital effects” in tropical corals: A new geochemical tool for probing biomineralization. *Geochim. Cosmochim. Acta* 69, 3265–3284.

Sinclair, D., Kinsley, L., McCulloch, M., 1998. High resolution analysis of trace elements in corals by laser ablation ICP-MS. *Geochim. Cosmochim. Acta* 62, 1889–1901.

Sorokin, Y.I., 1991. Biomass, metabolic rates and feeding of some common reef Zoantharians and Octocorals. *Aust. J. Mar. Freshwater Res.* 42, 729–741.

Stambler, N., Popper, N., Dubinsky, Z., Stimson, J., 1991. Effects of nutrient enrichment and water motion on the coral *Pocillopora damicornis*. *Pac. Sci.* 45, 299–307.

Standish, C.D., Chalk, T.B., Babila, T.L., Milton, J.A., Palmer, M.R., Foster, G.L., 2019. The effect of matrix interferences on in situ boron isotope analysis by laser ablation multi-collector inductively coupled plasma mass spectrometry. *Rapid Commun. Mass Spectrom.* 33, 959–968.

Growth and metabolic responses of *Acropora palifera* to long term nutrient enrichment Vol. 1, 1997, 867–872.

Stewart, J.A., Anagnostou, E., Foster, G.L., 2016. An improved boron isotope pH proxy calibration for the deep-sea coral *Desmophyllum dianthus* through sub-sampling of fibrous aragonite. *Chem. Geol.* 447, 148–160.

Sun, C.-Y., Stifler, C.A., Chopdekar, R.V., Schmidt, C.A., Parida, G., Schoeppler, V., Fordyce, B.I., Brau, J.H., Mass, T., Tambutte, S., Gilbert, P.U.P.A., 2020. From particle attachment to space-filling coral skeletons. *PNAS* 117, 2020–2025.

Szmant, A.M., 2002. Nutrient enrichment on coral reefs: is it a major cause of coral reef decline? *Estuaries* 25, 743–766.

Szmant, A.M., Forrester, A., 1996. Water column and sediment nitrogen and phosphorus distribution patterns in the Florida Keys, USA. *Coral Reefs* 15, 21–41.

Tambutté, E., Allemand, D., Zoccola, D., Meibom, A., Lotto, S., Caminiti, N., Tambutté, S., 2007. Observations of the tissue-skeleton interface in the scleractinian coral *Stylophora pistillata*. *Coral Reefs* 26, 517–529.

Tambutte, E., Tambutte, S., Segonds, N., Zoccola, D., Venn, A., Erez, J., Allemand, D., 2012. Calcein labelling and electrophysiology: insights on coral tissue permeability and calcification. *Proc. R. Soc. B* 279, 19–27.

Thompson, D.M., 2022. Environmental records from coral skeletons: A decade of novel insights and innovation. *Wiley Interdiscip. Rev. Clim. Change* 13, e745.

Tomascik, T., Sander, F., 1985. Effects of eutrophication on reef-building corals. *Mar. Biol.* 87, 143–155.

Tomascik, T., Sander, F., 1987. Effects of eutrophication on reef building corals. II: Structure of scleractinian coral communities on ringing reefs, Barbados. *West Indies. Mar. Biol.* 95, 53–75.

Ullman, W.J., Sandstrom, M.W., 1987. Dissolved Nutrient Fluxes from the Nearshore Sediments of Bowling Green Bay, Central Great Barrier Reef Lagoon (Australia). *Estuarine Coastal Shelf Sci.* 24, 289–303.

Wall, M., Fietzke, J., Crook, E.D., Paytan, A., 2019. Using B isotopes and B/Ca in corals from low saturation springs to constrain calcification mechanisms. *Nat. Commun.* 10, 3580.

Watanabe, T., Winter, A., Oba, T., 2001. Seasonal changes in sea surface temperature and salinity during the Little Ice Age in the Caribbean Sea deduced from Mg/Ca and  $^{18}\text{O}/^{16}\text{O}$  ratios in corals. *Mar. Geol.* 173, 21–35.

Wei, G., McCulloch, M.T., Mortimer, G., Deng, W., Xie, L., 2009. Evidence for ocean acidification in the Great Barrier Reef of Australia. *Geochim. Cosmochim. Acta* 73, 2332–2346.

Wells, J.W., 1956. Scleractinia. In: Moore, R.C. (Ed.), *Treatise on invertebrate paleontology*, Part F. Geological Society of America, New York, pp. F328–F444.

Wiedenmann, J., D'Angelo, C., Smith, E.G., Hunt, A.N., Legiret, F.-E., Postle, A.D., Achterberg, E.P., 2013. Nutrient enrichment can increase the susceptibility of reef corals to bleaching. *Nat. Clim. Change* 3, 160–164.

Zeebe, R.E., Wolf-Gladrow, D.A., 2001.  $\text{CO}_2$  in Seawater: Equilibrium, Kinetics, Isotopes. Elsevier, Amsterdam.

Zoccola, D., Ganot, P., Bertucci, A., Caminiti-Segonds, N., Techer, N., Voolstra, C.R., Aranda, M., Tambutté, E., Allemand, D., Casey, J.R., Tambutté, S., 2015. Bicarbonate transporters in corals point towards a key step in the evolution of cnidarian calcification. *Sci. Rep.* 5, 9983.